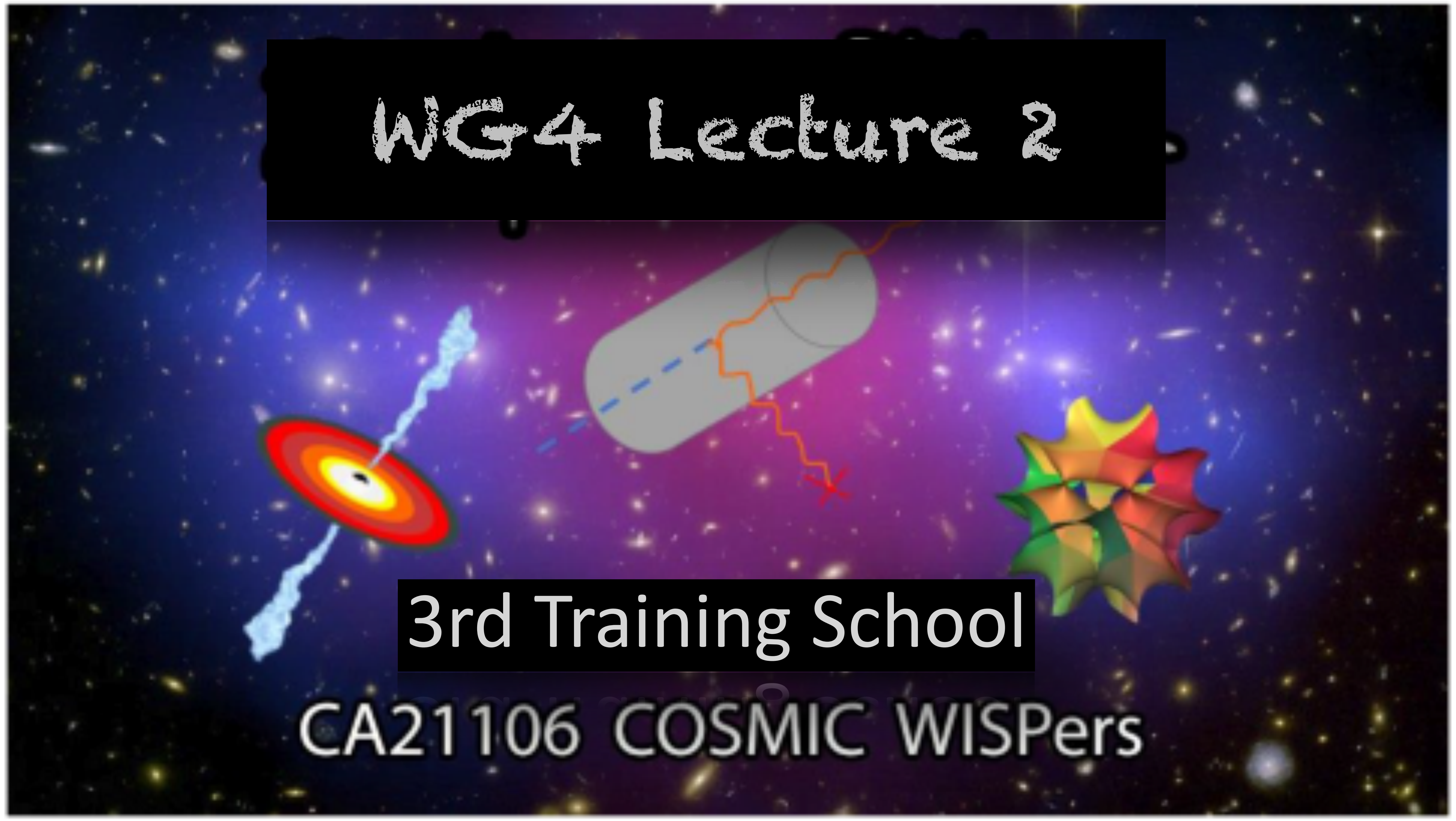

Probing ultralight axion-like particles with quantum technology

Sreemanti Chakraborti

COSMIC WISPERS CA21106
cost EUROPEAN COOPERATION IN SCIENCE & TECHNOLOGY
Funded by the European Union
UNIVERSITÉ SAVOIE MONT BLANC
cnrs
LAPTh Laboratoire d'Annecy de Physique Théorique
Durham University
IP3

Resonant Cavities

Cavity Haloscopes

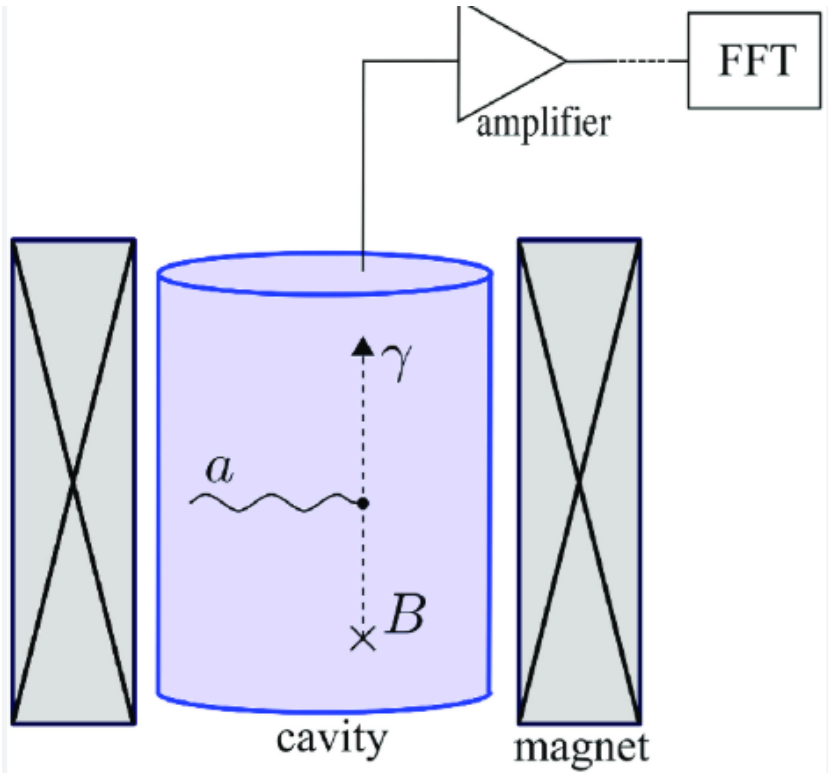

- Haloscopes are microwave cavities tuned to detect the resonant conversion of dark matter ALPs into photons in the presence of a strong static magnetic field
- ALP conversion takes place through **Inverse Primakoff production** which is primarily induced by the linear ALP-photon interaction

$$\boxed{g_{a\gamma\gamma} \frac{a}{4} F_{\mu\nu} \tilde{F}^{\mu\nu} = g_{a\gamma\gamma}\, a \vec{E} \cdot \vec{B}}$$

- In a resonant microwave cavity immersed in a magnetic field, axions interact with the virtual photons of the magnetic field and convert to an oscillating electromagnetic field.
- The ALP conversion maximises if its Compton frequency matches the frequency of a resonant mode of the cavity resonator.

Sikivie Phys. Rev. D 32, 2988 (1985)

Kimball *et. al,* The Search for Ultralight Bosonic Dark Matter

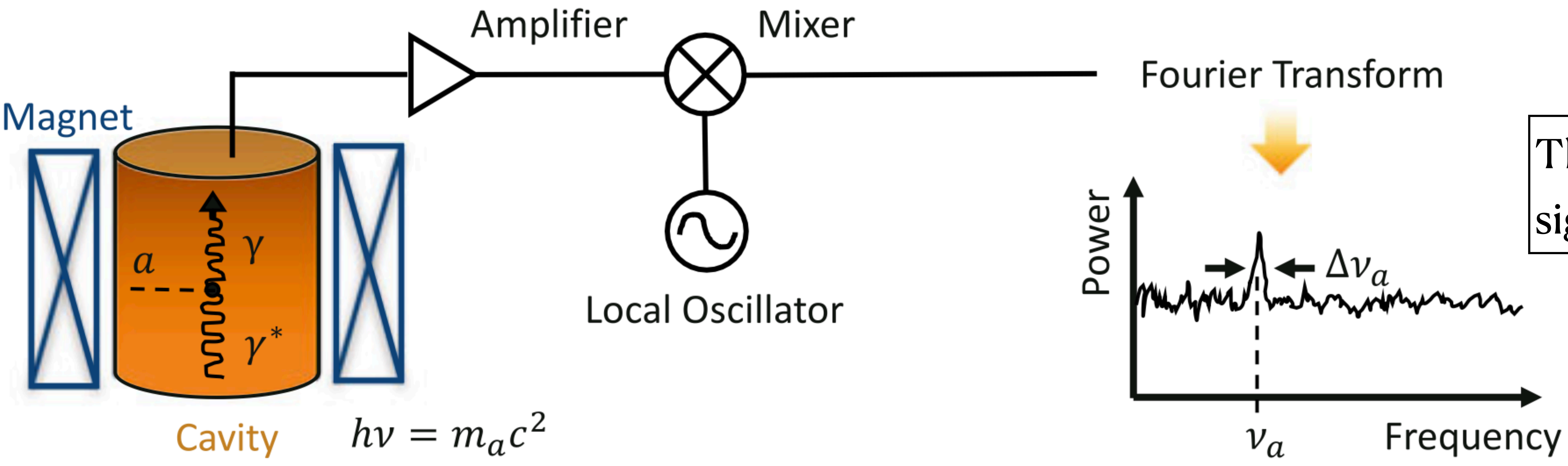

The width of the axion signal $\sim \Delta\nu_a \lesssim 10^{-6}\,\nu_a$

- The resonant conversion condition is that the ALP mass is within the bandwidth of the microwave cavity at its resonance frequency.
- Since the axion mass is unknown, the cavity resonance frequency must be tuned to access a range of axion masses.
- Photons generated from ALP-photon conversion give rise to excess power generation inside the cavity. The frequency dependent signal power extracted on resonance-

$$\boxed{P_{a\to\gamma} = g_{a\gamma\gamma}^2 \frac{\rho_{\rm DM}}{m_a} B_0^2 V C \min(Q_L, Q_a)}$$

Key scaling relations

- Signal power depends on:

$$P \sim g_{a\gamma}^2 \, \rho_a \, B^2 \, V \, C \, Q$$

- **B field**: stronger magnets = stronger signal
- **V**: larger cavities for lower masses
- **Q**: sharp resonances, limited by material losses

Trade-offs : Large volume vs. High frequency

Experimental implementations

◉ **ADMX** (pioneering, μeV range)

◉ **HAYSTAC** (quantum-limited amplifiers, squeezed states)

◉ **ADMX-SLIC (**Tunable LC circuits, lighter mass**)**

◉ **ADMX-SIDECAR, ORGAN (**tunable to higher cavity modes, heavier masses)

◉ **QUAX** (Ferromagnetic haloscopes exploiting the principle of magnetic resonances)

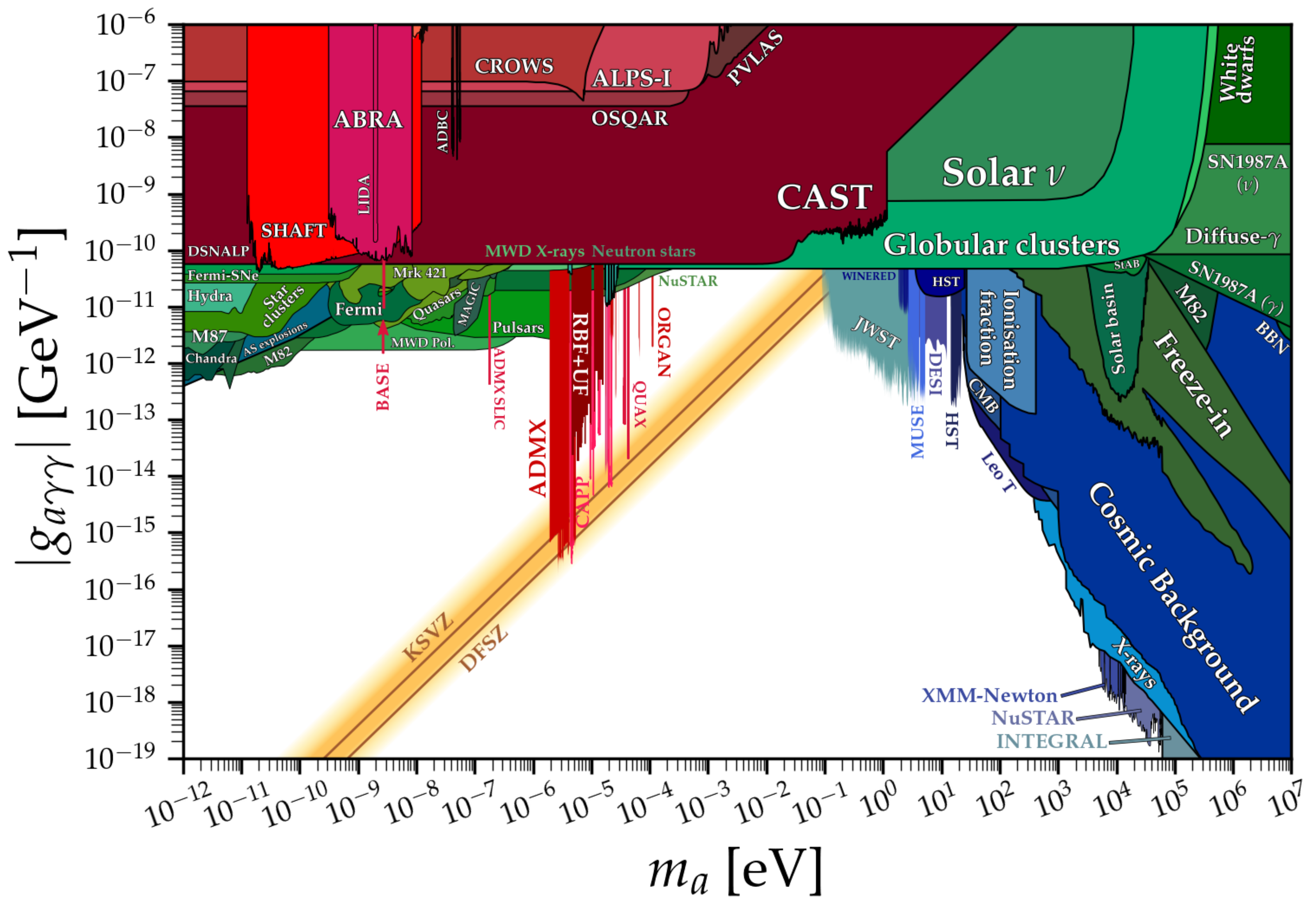

Next generation innovations

MADMAX (dielectric haloscope): stacked dielectric disks

Constructive interference of coherent photon emission at several interfaces

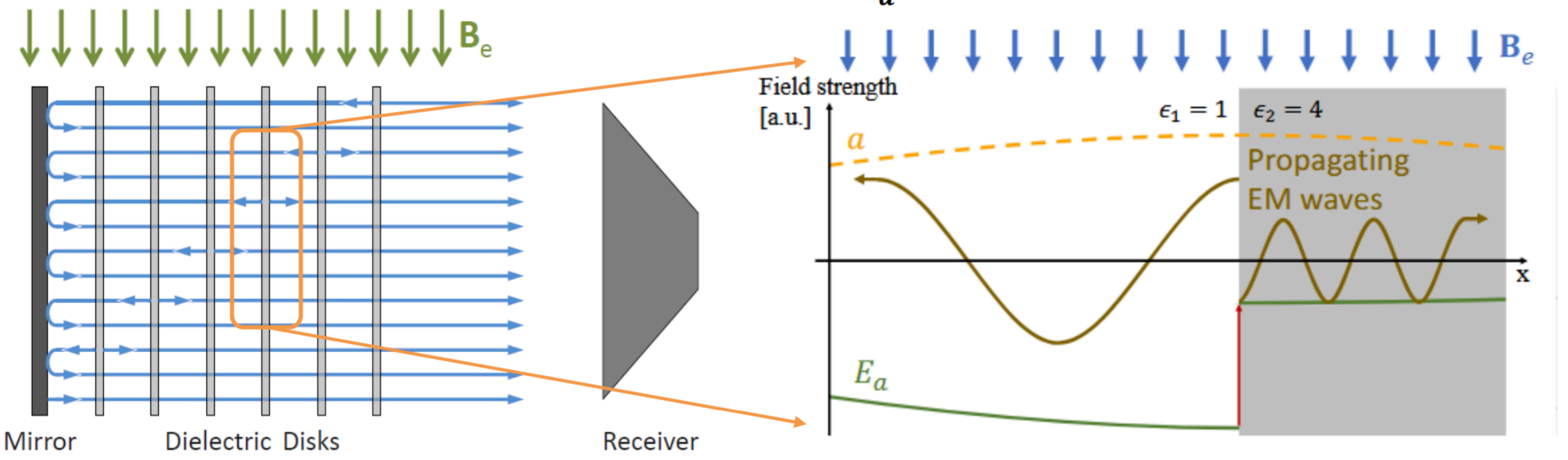

MADMAX PRL118 (2017) 091801

At the surface, $E_{\parallel}$ must be continuous
→ Coherent emission of electromagnetic waves

proposed to probe a up to a few orders above the $\mu\mathrm{eV}$ scale

Next generation innovations

SRF Cavities: superconducting resonant frequency conversion

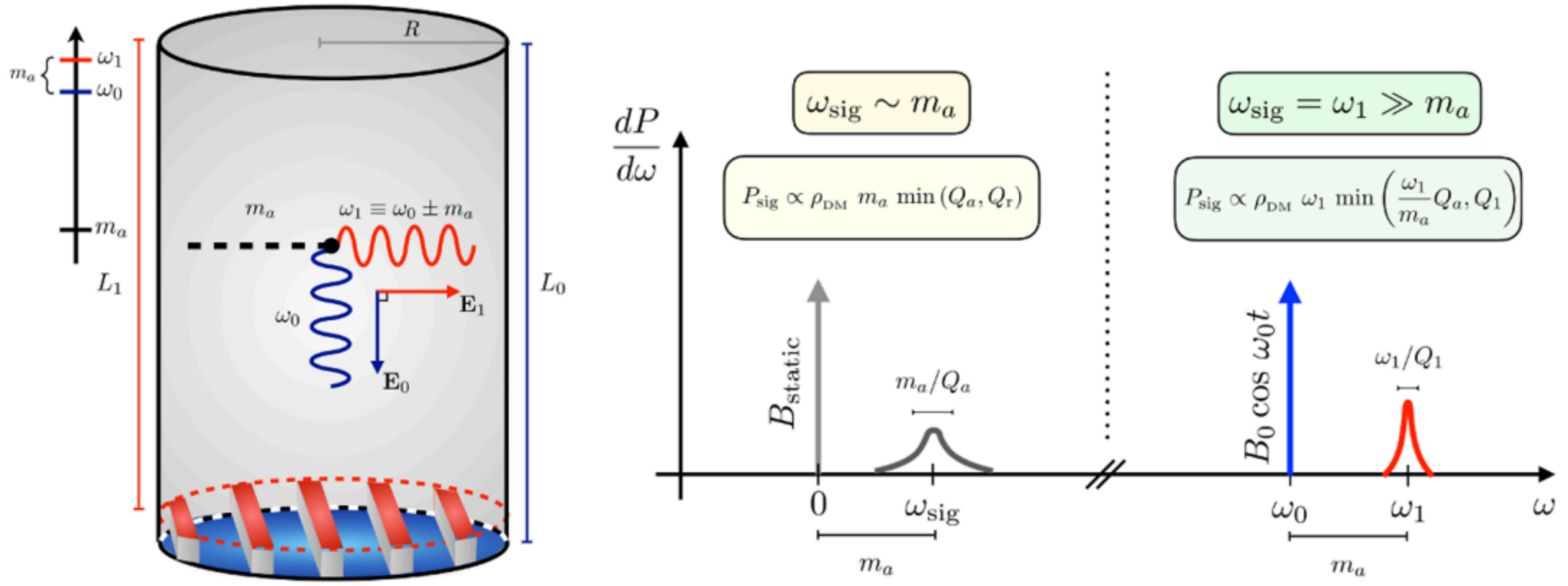

(a) Cartoon of cavity setup.

(b) Signal parametrics.

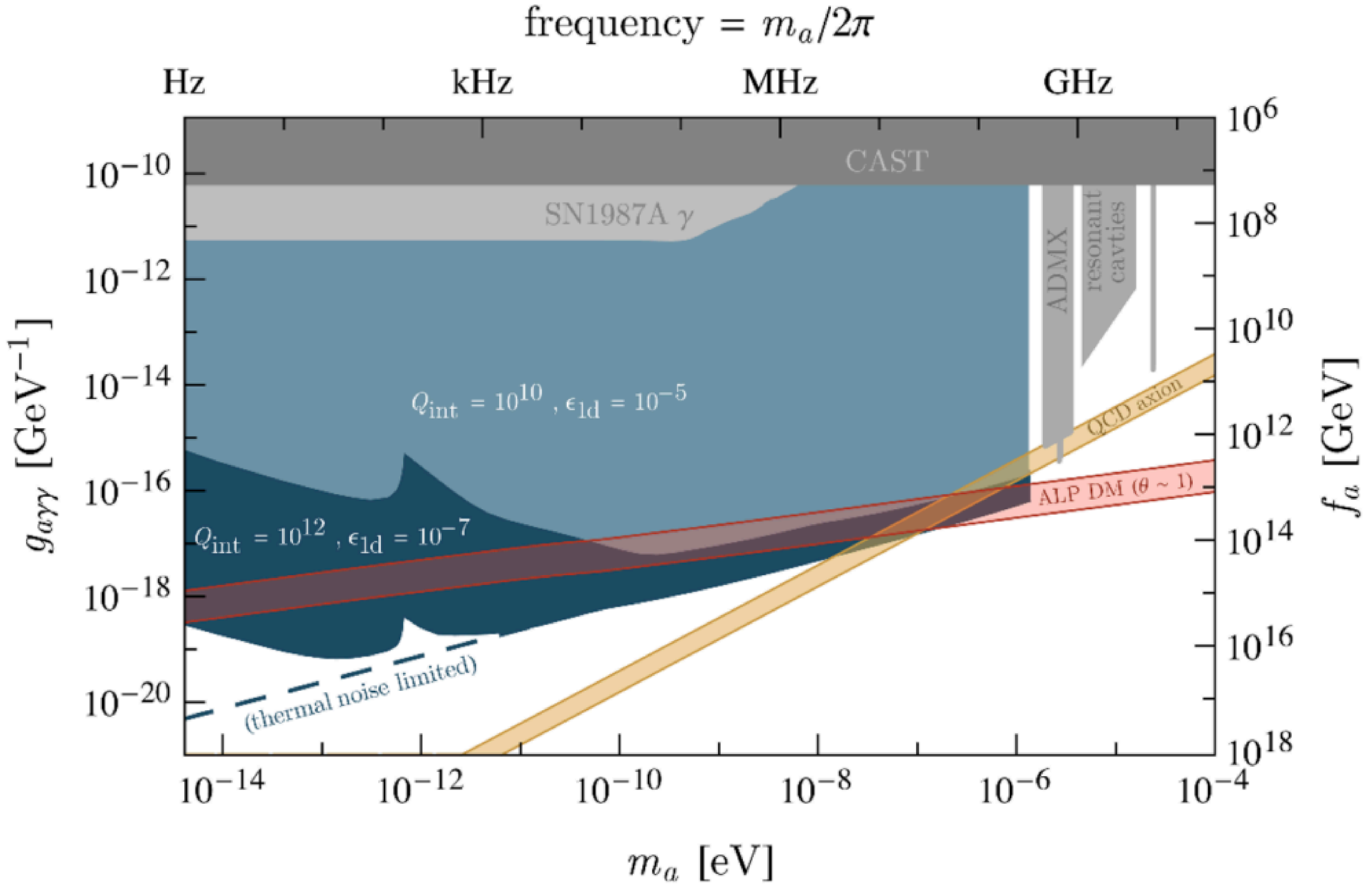

Cavities with much higher quality factor, $Q \sim 10^9$

Berlin et. al : JHEP07(2020)088

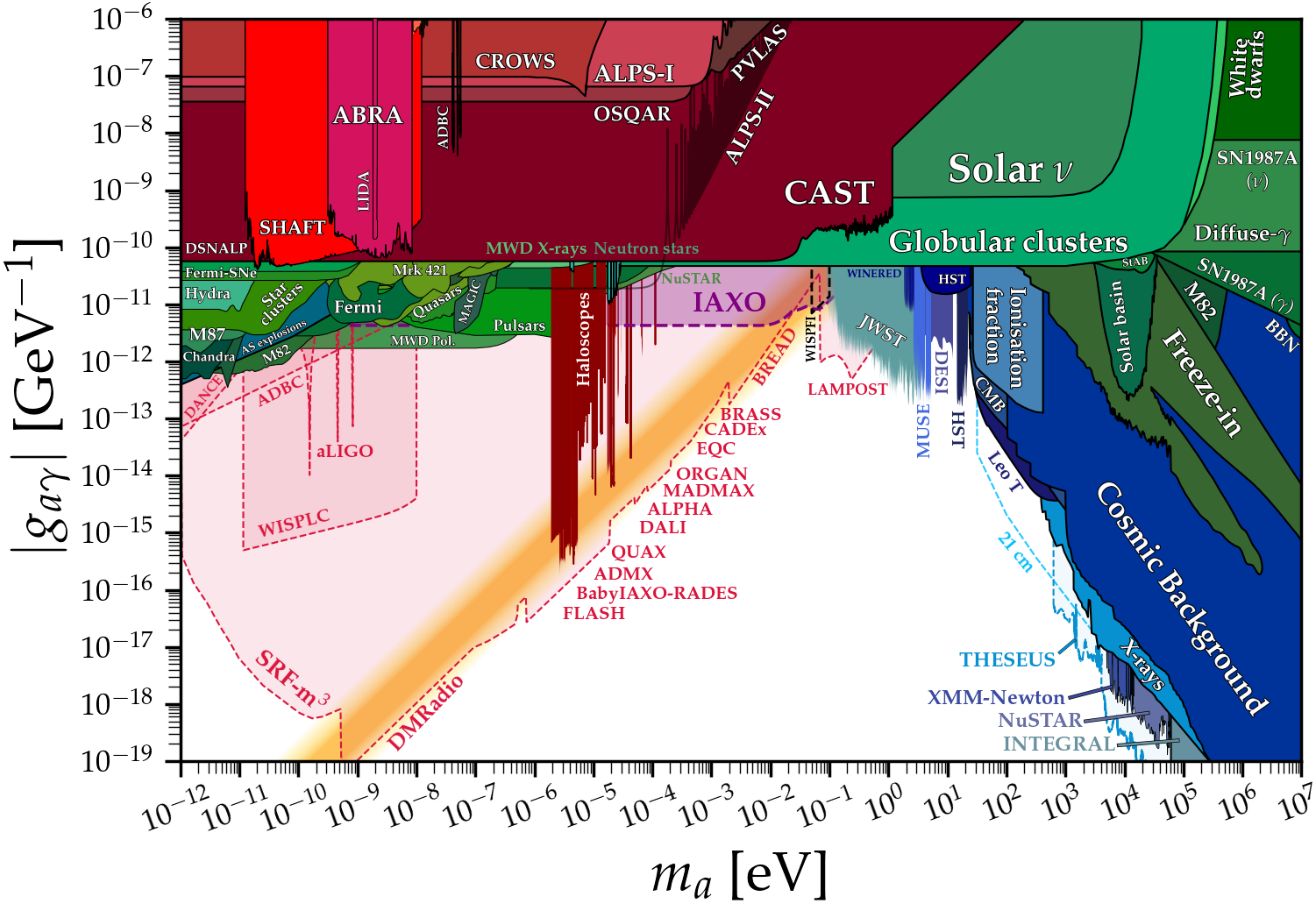

CROWS
ALPS-I
PVLAS
ABRA
OSQAR
ALPS-II
ADBC
LIDA
CAST
Solar ν
White dwarfs
SN1987A (ν)
SHAFT
Globular clusters
Diffuse-γ
DSNALP
MWD X-rays
Neutron stars
Fermi-SNe
Mrk 421
NuSTAR
WINERED
HST
StAB
SN1987A (γ)
Hydra
Star clusters
Fermi
Quasars
MAGIC
Haloscopes
IAXO
JWST
Ionisation fraction
Solar basin
M82
BBN
M87
AS explosions
Pulsars
WISPFI
Freeze-in
Chandra
M82
MWD Pol.
BREAD
DESI
DANCE
ADBC
LAMPOST
CMB
BRASS
CADEx
EQC
MUSE
HST
aLIGO
ORGAN
MADMAX
ALPHA
DALI
Leo T
WISPLC
QUAX
ADMX
BabyIAXO-RADES
FLASH
21 cm
Cosmic Background
X-rays
THESEUS
XMM-Newton
NuSTAR
INTEGRAL
SRF-m³
DMRadio
$|g_{a\gamma}|$ [GeV^{-1}]
m_a [eV]

Helioscopes

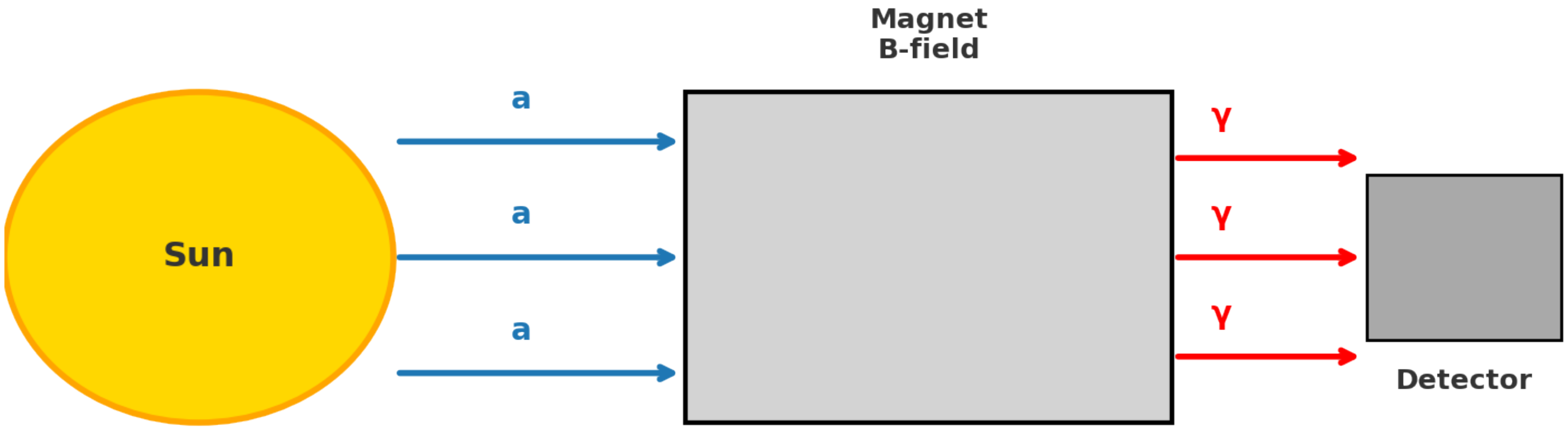

Inside the sun

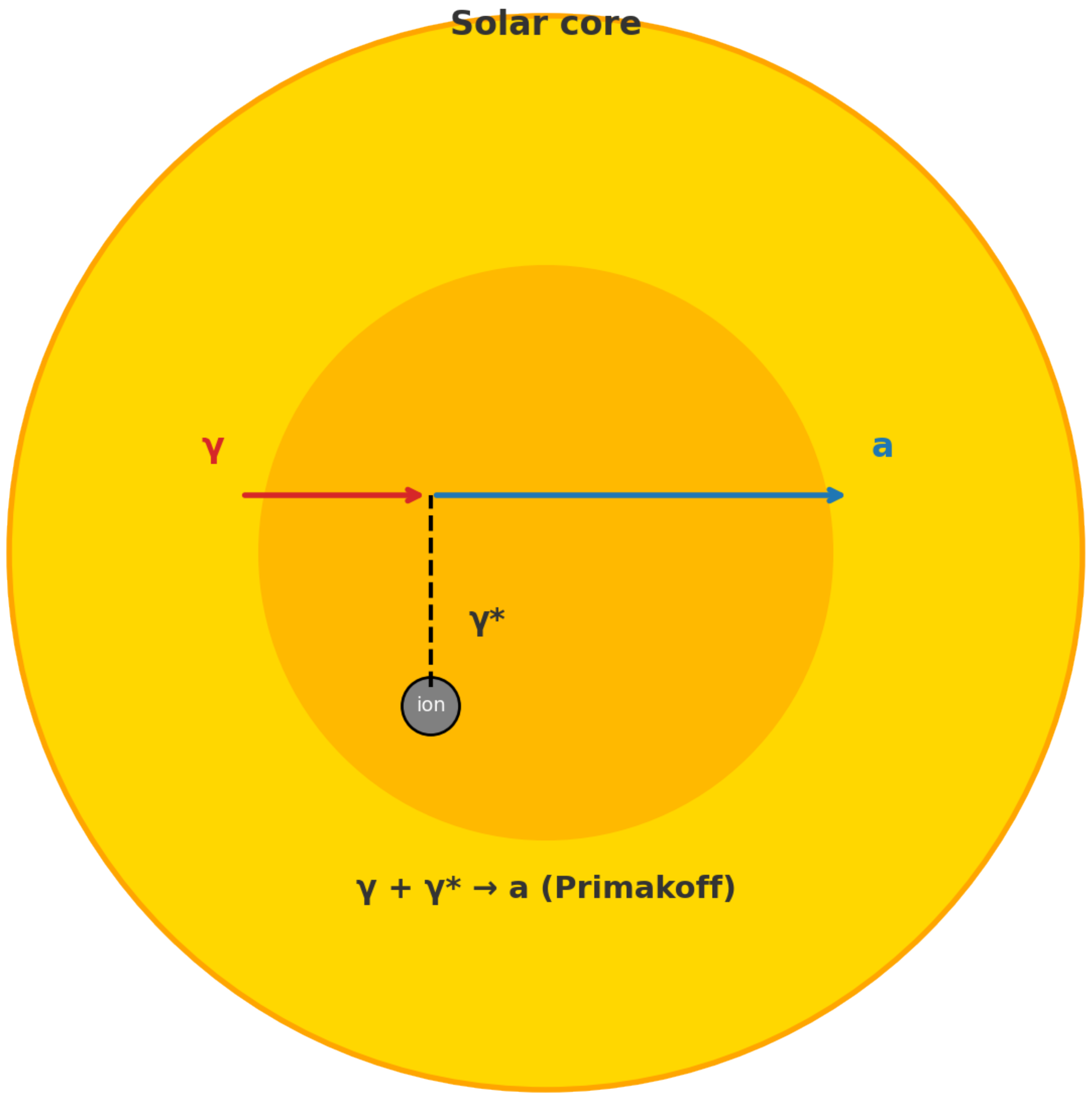

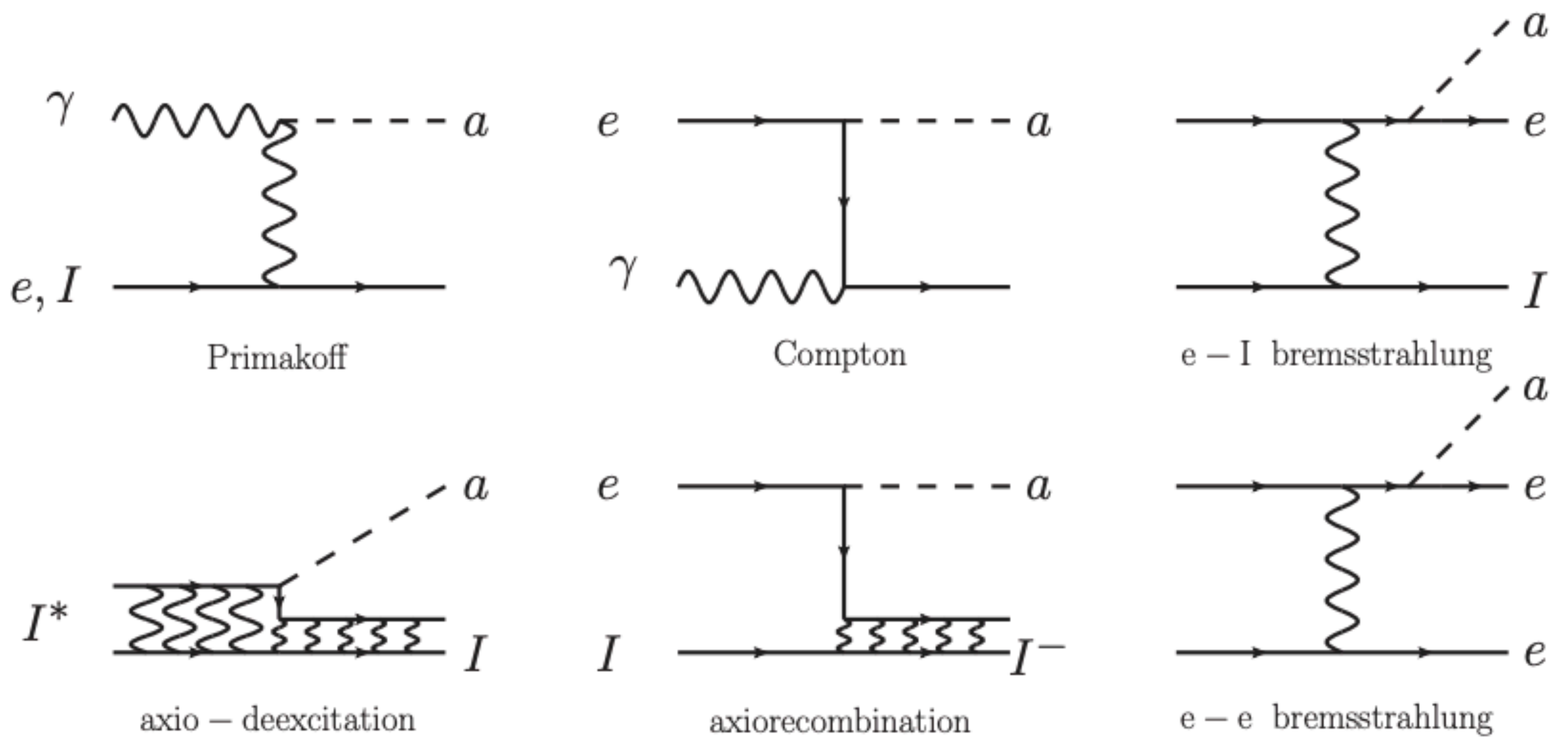

Fluxes

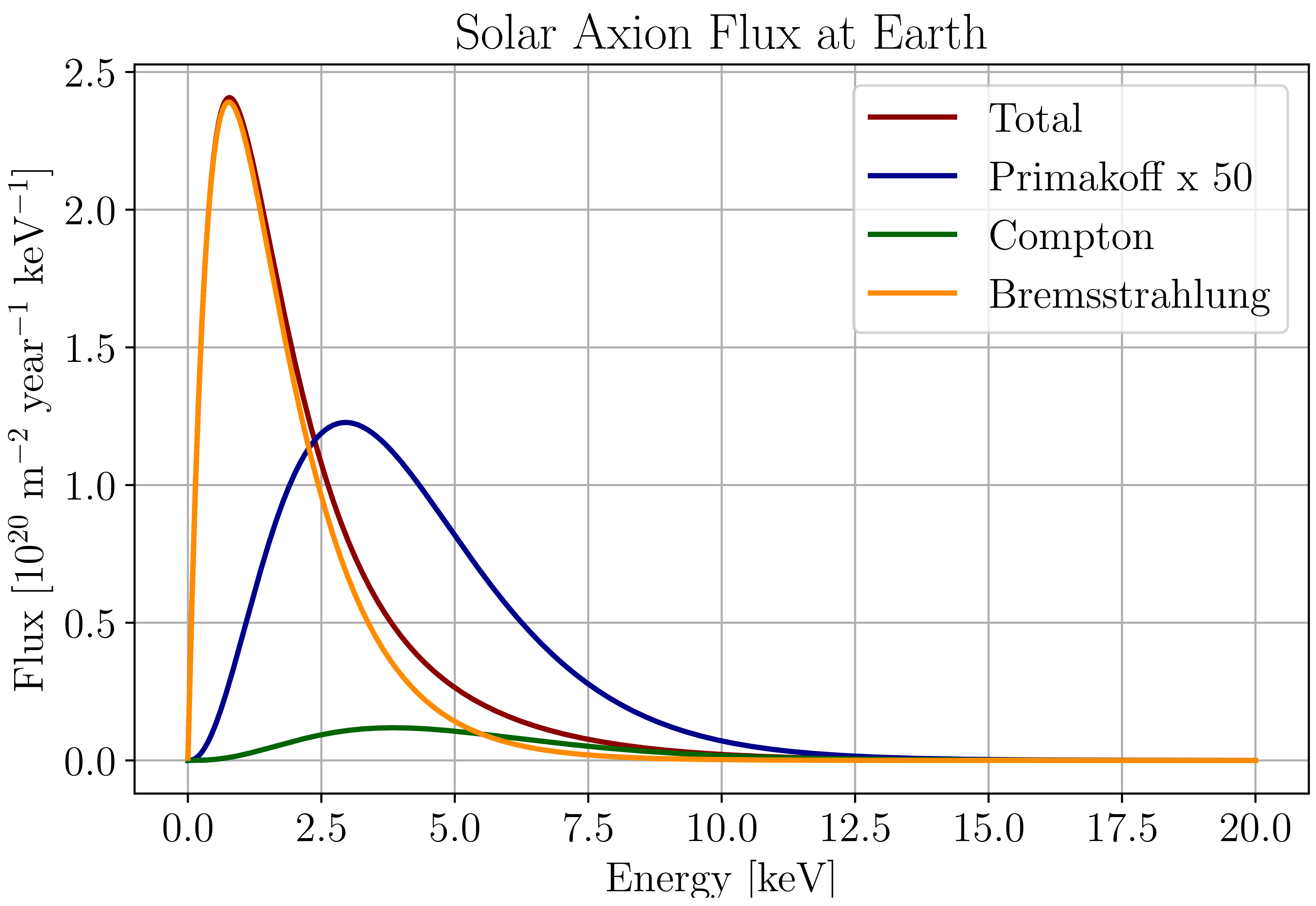

$$\left.\frac{\mathrm{d}\Phi_a}{\mathrm{d}\omega}\right|_P = 2.0\times10^{18}\left(\frac{g_{a\gamma}}{10^{-12}\mathrm{GeV}^{-1}}\right)^2\omega^{2.450}\,e^{-0.829\,\omega}$$

$$\left.\frac{\mathrm{d}\Phi_a}{\mathrm{d}\omega}\right|_C = 4.2\times10^{18}\left(\frac{g_{ae}}{10^{-13}}\right)^2\omega^{2.987}\,e^{-0.776\,\omega}$$

$$\left.\frac{\mathrm{d}\Phi_a}{\mathrm{d}\omega}\right|_B = 8.3\times10^{20}\left(\frac{g_{ae}}{10^{-13}}\right)^2\frac{\omega}{1+0.667\,\omega^{1.278}}\,e^{-0.77\,\omega}$$

Axions Escape the Sun Freely

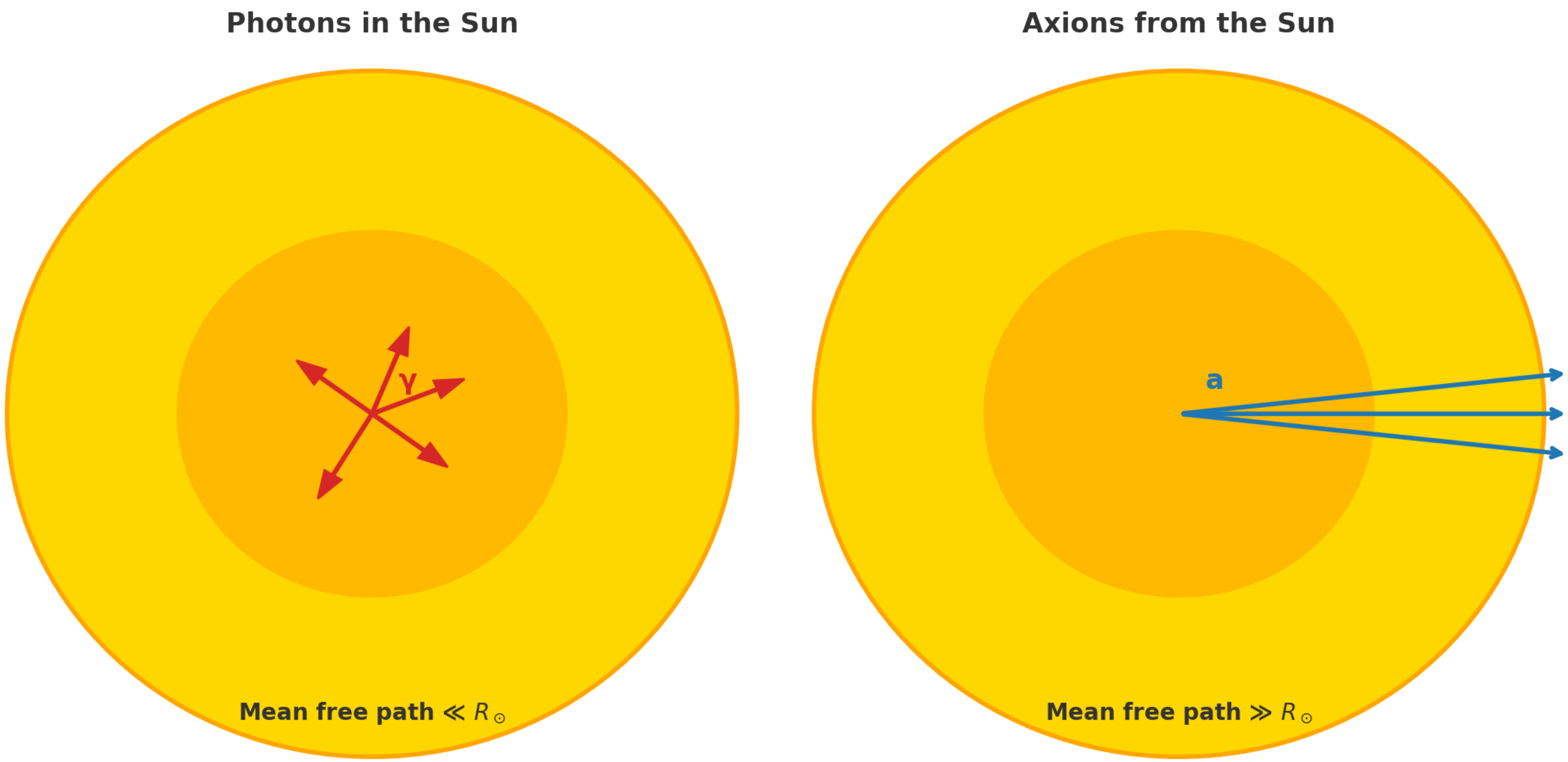

$$\ell_a \approx 6\times 10^{24}\, g_{10}^{-2}\,\mathrm{cm}$$
$$\approx 8\times 10^{13}\, g_{10}^{-2}\, R_\odot$$

For $g_{a\gamma} = 10^{-10}\,\mathrm{GeV}^{-1}$:
$\ell_a \sim 10^{14}\, R_\odot$ (free streaming)

$g_{a\gamma}$ needs to be $\sim 10^7$ larger

to get reabsorbed in the sun !!!

Why Solar Axion Signals Are Clean on Earth

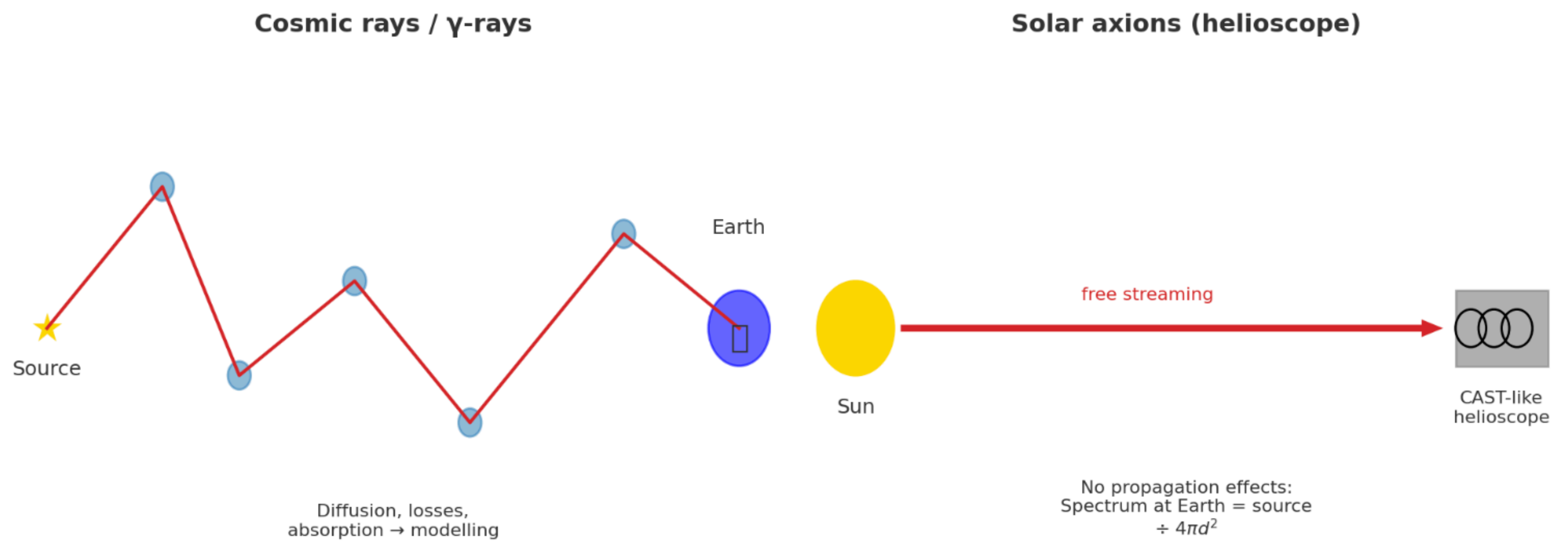

Inside a helioscope

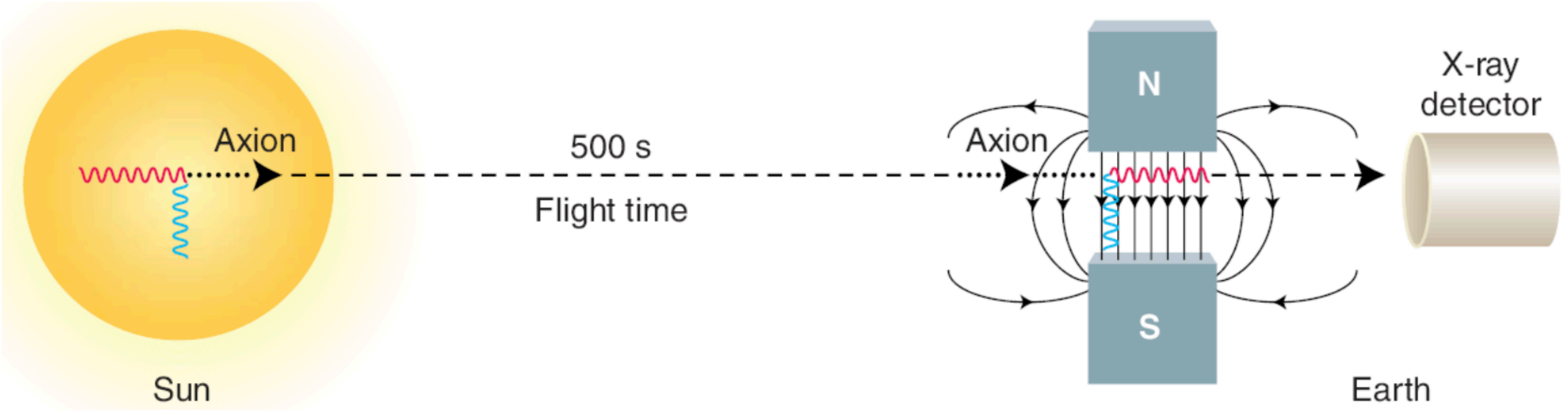

- **Conversion:** Axions → X-rays via *inverse Primakoff* in strong transverse B
- **Photon energy:** Matches solar production spectrum (few keV)
- **Detectors:**
  - *CCDs*— pixel imaging, keV sensitivity
  - *Micromegas/TPCs* — gaseous, strong background rejection
  - *Cryogenic calorimeters* — high resolution, low thresholds
- **Background control :** shielding, anticoincidence, low-noise setups

Coherence

$$P_{a\to\gamma} = \left(\frac{BLg_{a\gamma\gamma}}{2}\right)^2 \left(\frac{\sin\left(\frac{qL}{2}\right)}{\left(\frac{qL}{2}\right)}\right)^2, \quad q \simeq \frac{|m_a^2 - m_\gamma^2|}{2E} = k_a - k_\gamma$$

Coherence condition: $\frac{qL}{2} \lesssim \pi$

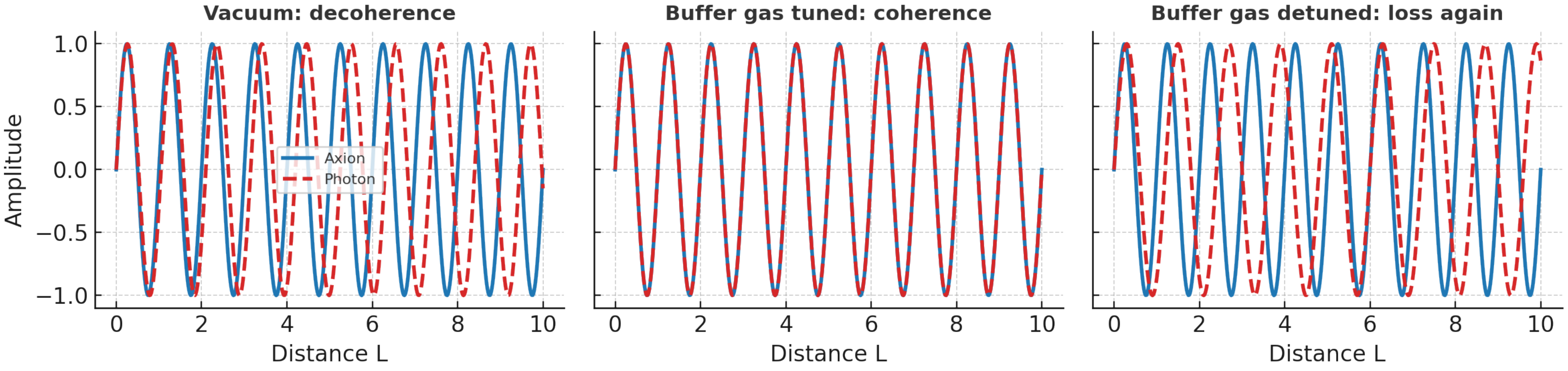

$$N_\gamma = \int_E \frac{d\Phi\left(E_a, g_{a\gamma\gamma}^2\right)}{dE_a} P_{a\to\gamma}\left(E_a, m_a, g_{a\gamma\gamma}^2\right) \epsilon\left(E_a\right)\ \Delta t\ A\ dE_a$$

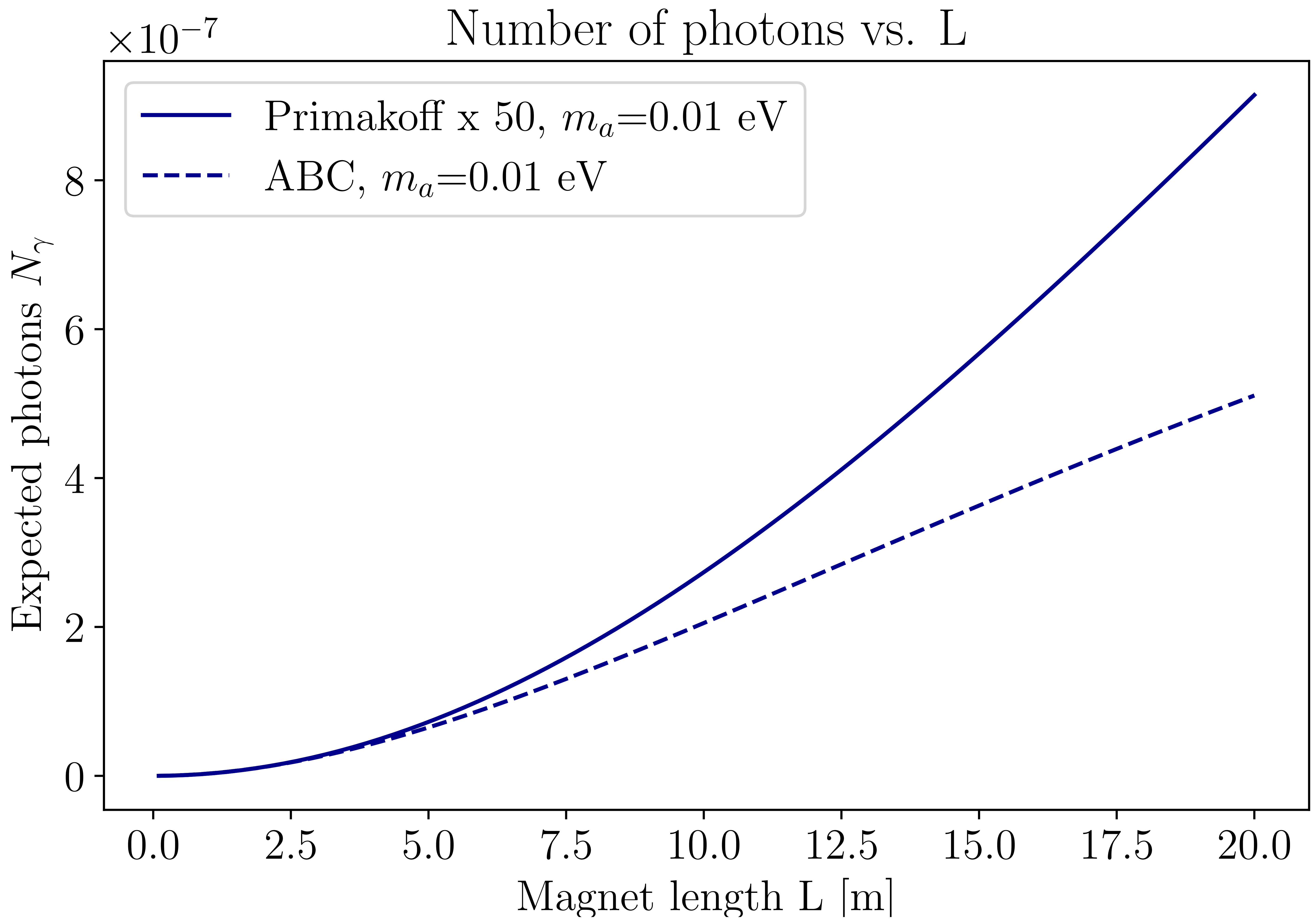

Buffer gas

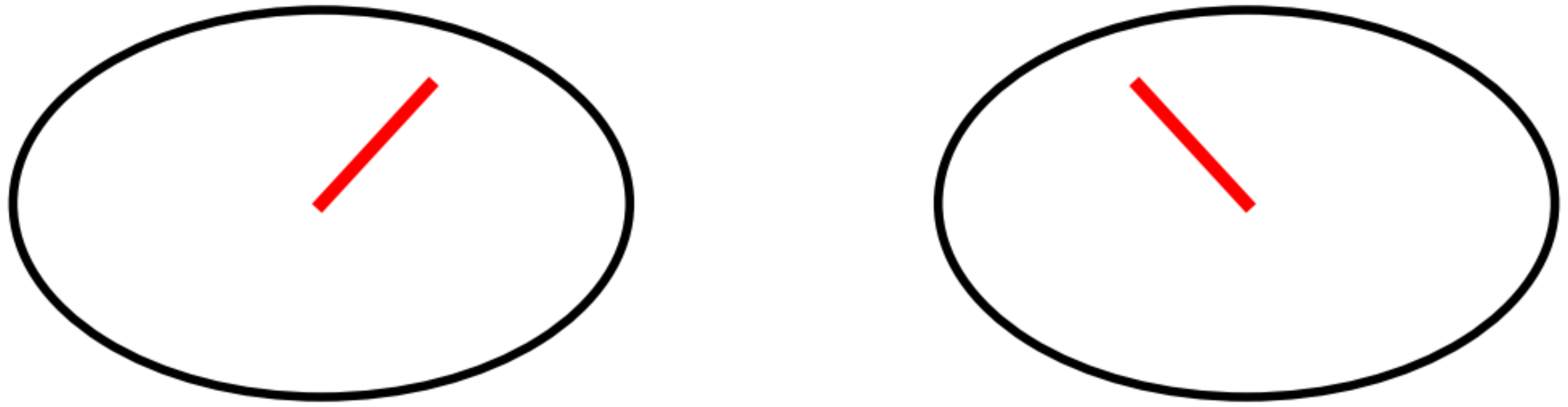

He-4
(low mass up to ~0.4 eV)

He-3
(high mass up to ~1.2 eV)

$$\Delta m_\gamma \lesssim \frac{2\pi E}{L m_a}$$

$$\Delta P = \frac{\Delta m_\gamma}{m_\gamma} P$$

Each pressure step → small axion mass interval

Step 1	Step 2	Step 3	Step 4	Step 5	Step 6	...	Step N (hundreds)

CAST-CERN Axion Solar Telescope

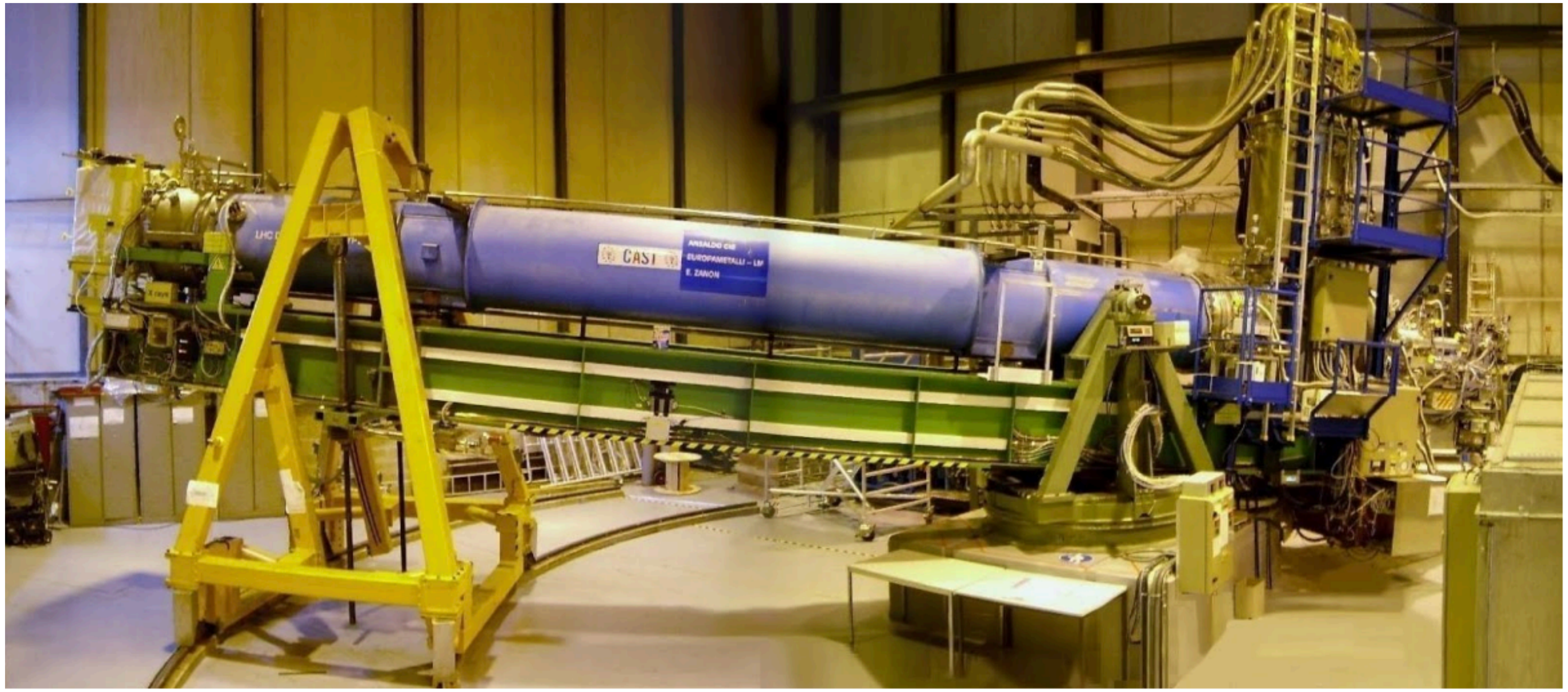

CAST collaboration, Nature Phys. 13 (2017) 584–590

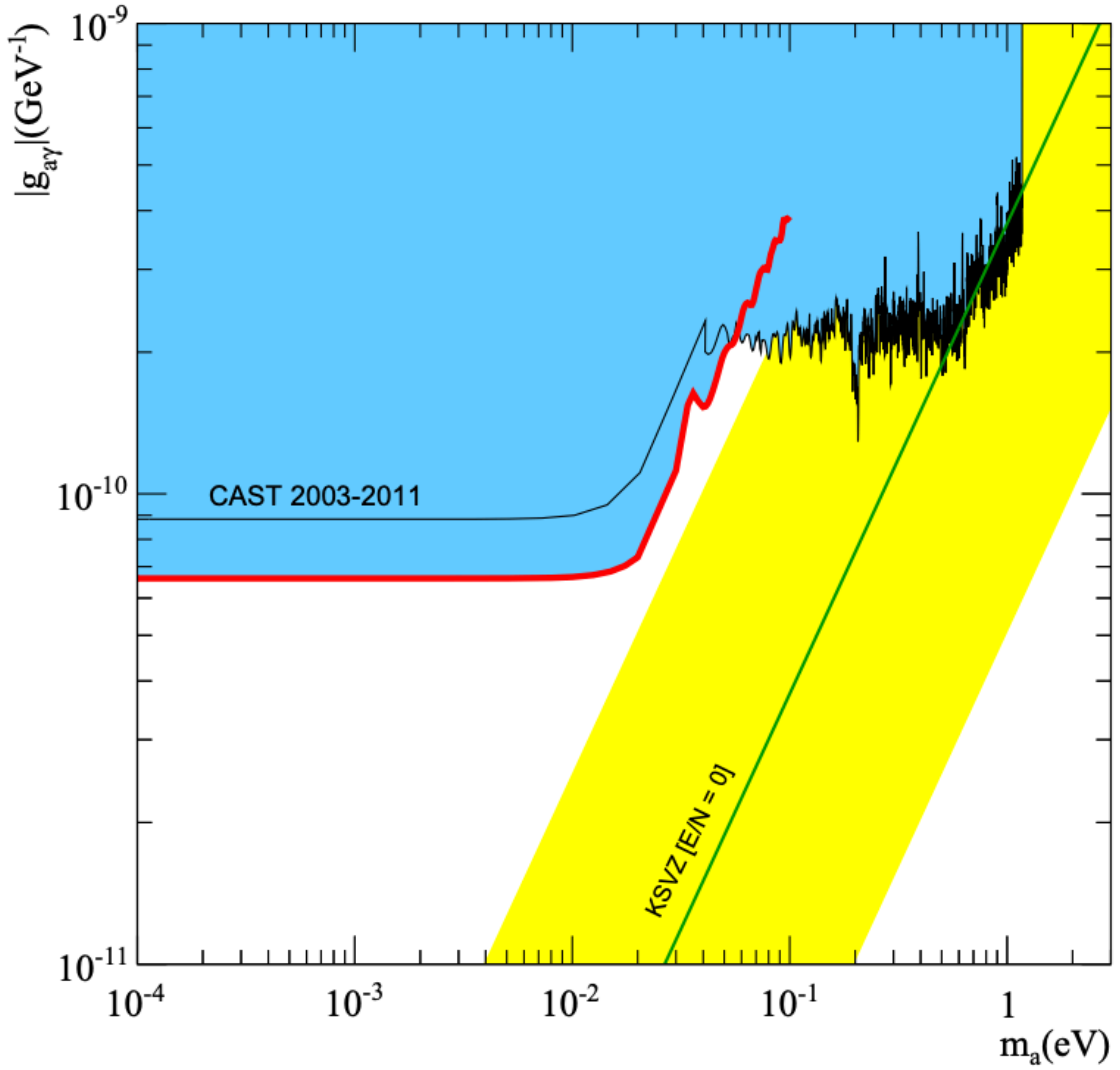

Magnet: LHC dipole magnets, B= 9T, L= 9.3 m

Bores : 2x14.5 cm^2

Phases: I (vacuum), II (^{4}He, ^{3}He), 2 more until 2014

X-ray optics: CCD (ESA spare)

Detectors: Micromegas, TPC, others

The first helioscope to have crossed the KSVZ line

Signal: X-ray excess from focused solar axions

Background: low, dominated by noise and cosmic rays

Detector parameters

Detection Toolkit

B	magnetic field strength
L	magnet length
A	cross-sectional area
ϵ_d	detector efficiency
ϵ_0	optics throughput
ϵ_t	tracking efficiency
t	exposure time
b	background rate
a	optics spot size

$N_\gamma \propto B^2 L^2 A \epsilon\, t\, g^4$ → **Signal counts:** conversion, flux, efficiency, exposure

$N_b = b\, a\, \epsilon_t\, t$ → **Background counts:** rate, spot area, tracking, time

$$\mathrm{SNR} = \frac{N_\gamma}{\sqrt{N_b}}$$ → **Signal-to-noise ratio** (discovery potential)

$$g \sim \left(\frac{N^*}{\sqrt{N_b}}\right)^{-1/4}$$ → Coupling sensitivity from SNR scaling

Figure of merit

$$\boxed{f = \frac{N^*}{\sqrt{N_b}} = f_{\mathrm{M}}\, f_{\mathrm{DO}}\, f_{\mathrm{T}}}$$

$$f_{\mathrm{M}} = B^2 L^2 A \longrightarrow$$ Magnet strength and geometry

$$f_{\mathrm{DO}} = \frac{\epsilon_d\, \epsilon_0}{\sqrt{ba}} \longrightarrow$$ Detector+optics performance

$$f_{\mathrm{T}} = \sqrt{\epsilon_t\, t} \longrightarrow$$ Tracking efficiency and exposure

Figure of merit

$$f \sim (B^2\, L^2\, \mathbf{A}) \times \frac{\epsilon_d \epsilon_0}{\sqrt{ba}} \times \sqrt{\epsilon_t t}$$

Larger A → more signal photons

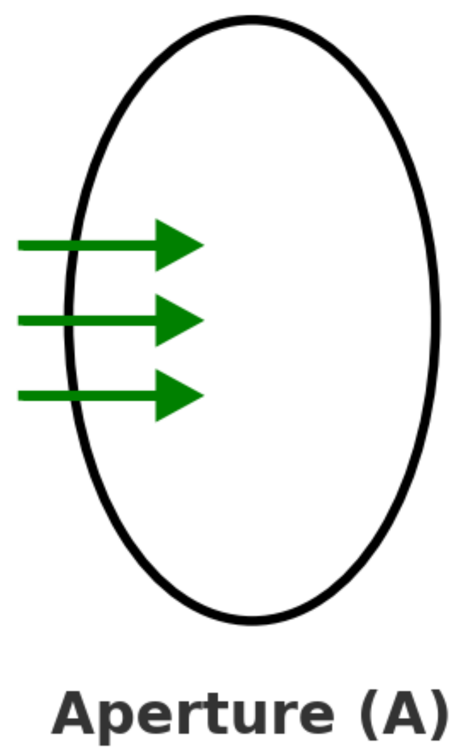

But also more background

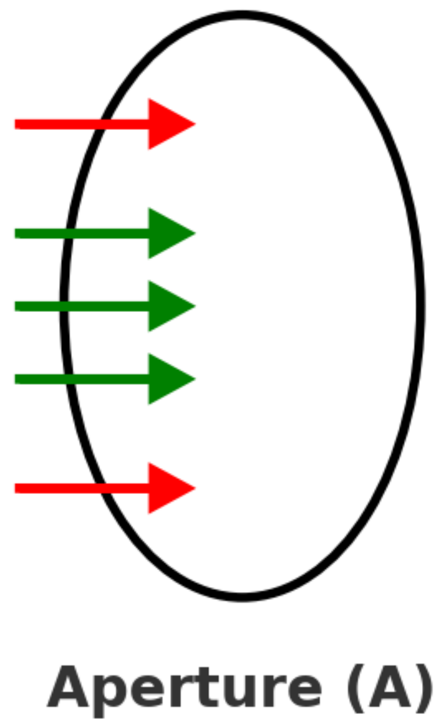

Optics: signal ∝ A,
background ∝ a

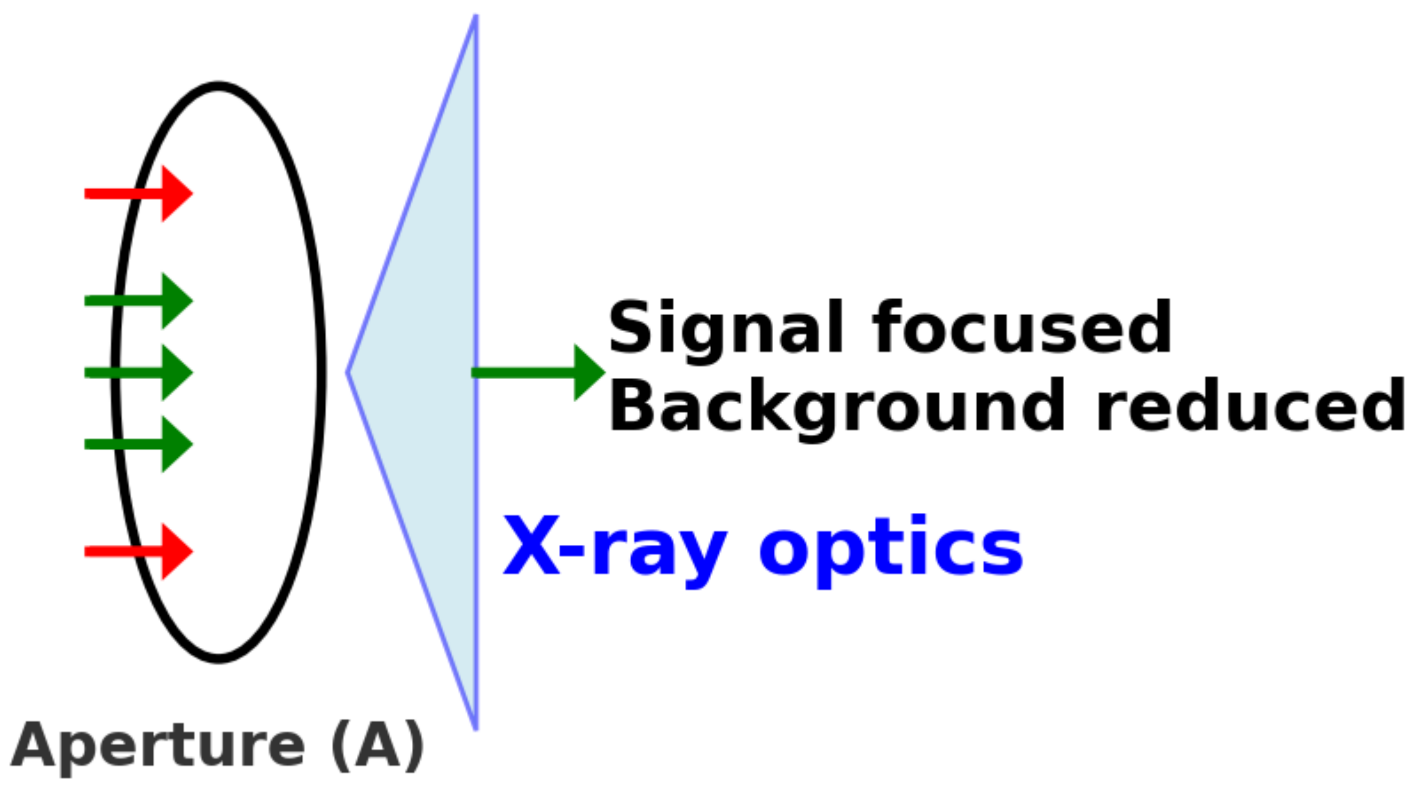

Figure of merit

$$f \sim \left(B^2 \mathbf{L^2} A\right) \times \frac{\epsilon_d \epsilon_0}{\sqrt{ba}} \times \sqrt{\epsilon_t t}$$

Larger L → more conversion

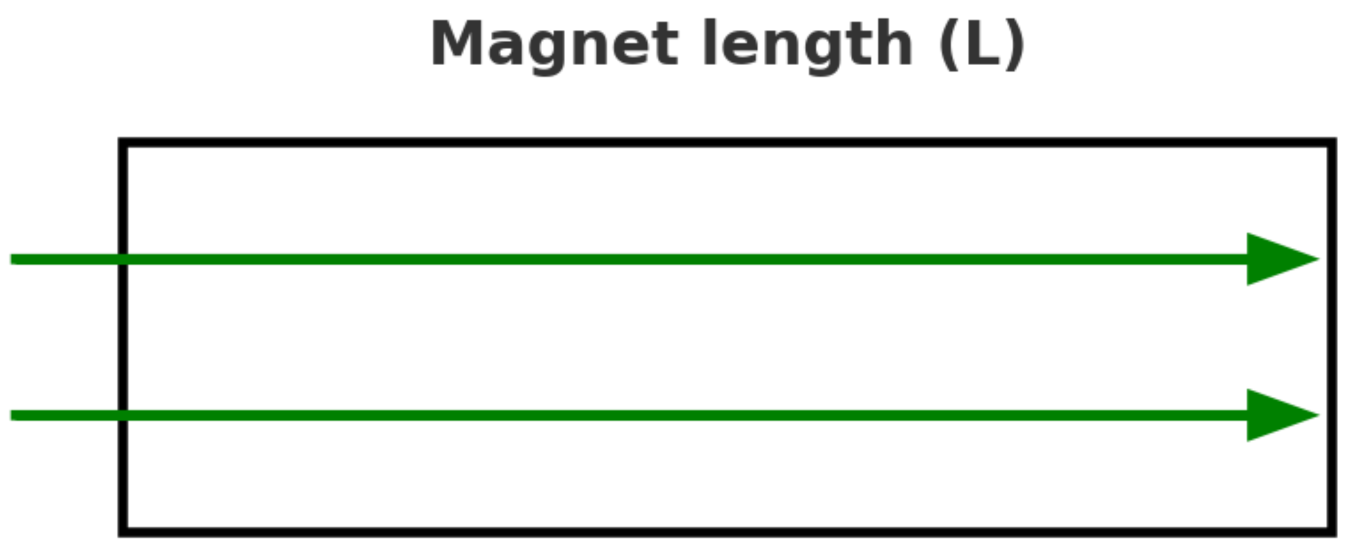

But decoherence occurs

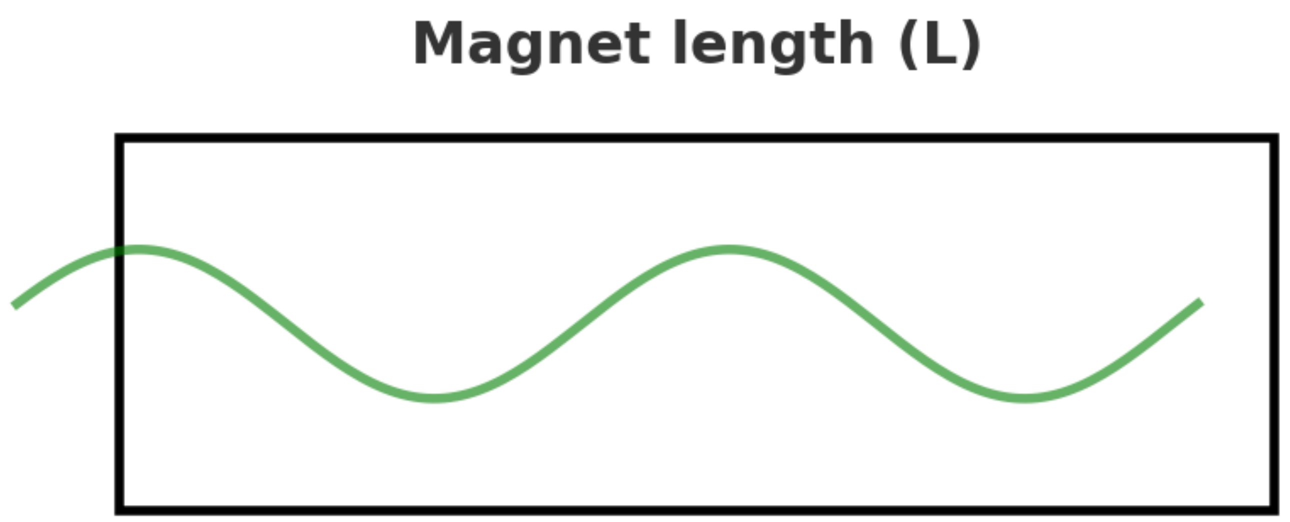

Buffer gas restores coherence

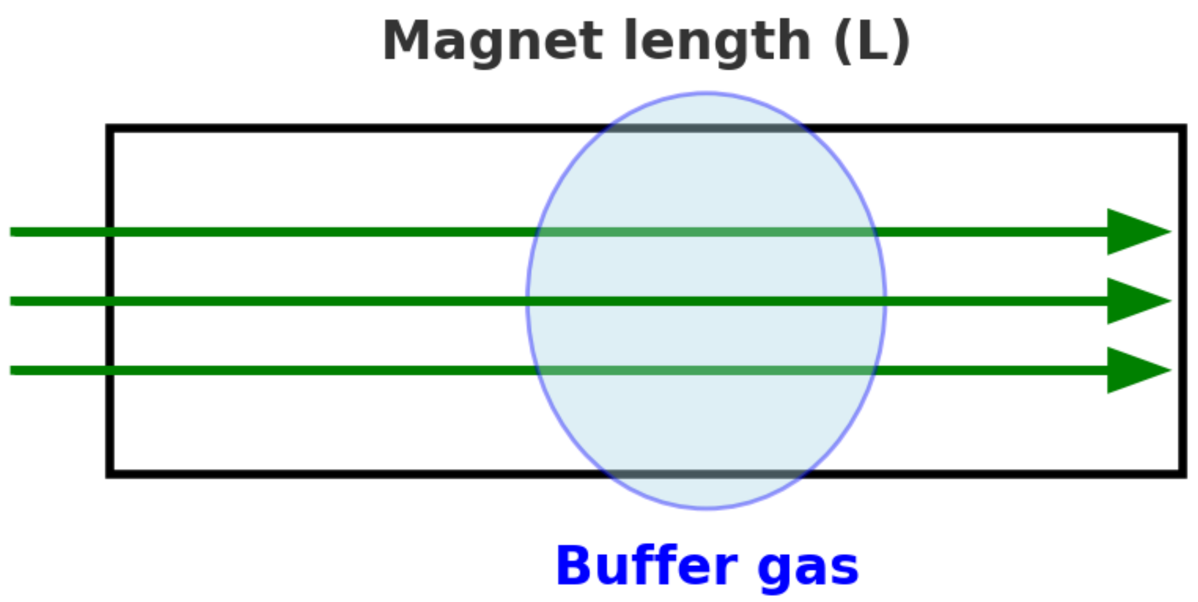

Figure of merit

$$f \sim \left(B^2 \; L^2 \; A\right) \times \frac{\epsilon_d \epsilon_0}{\sqrt{ba}} \times \sqrt{\epsilon_t t}$$

Increase B

Magnet field (B)

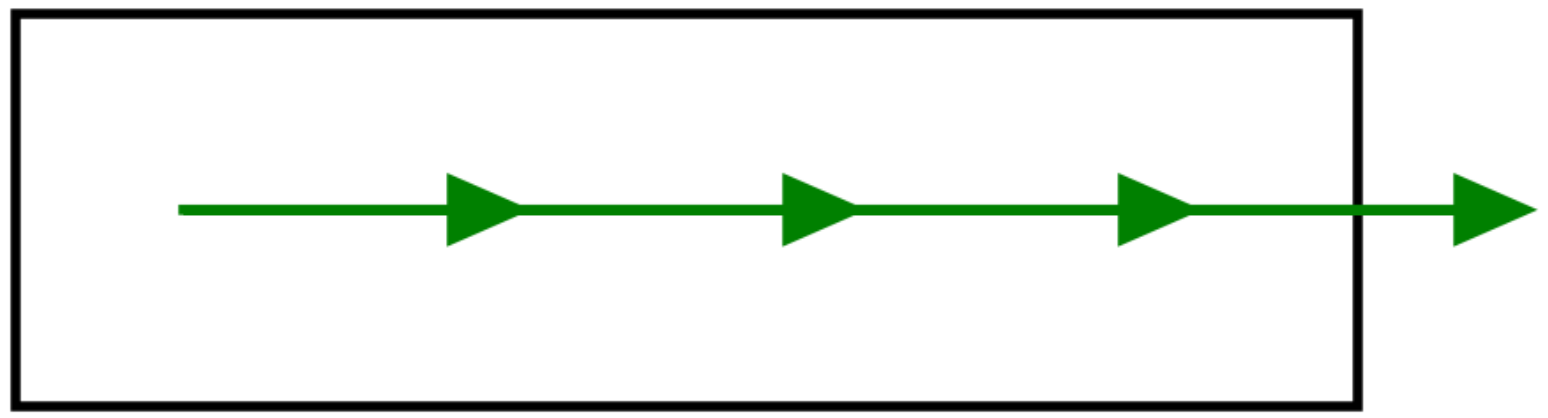

Stronger B → more photons (∝ B^2)

Limitations of large B

Magnet field (B)

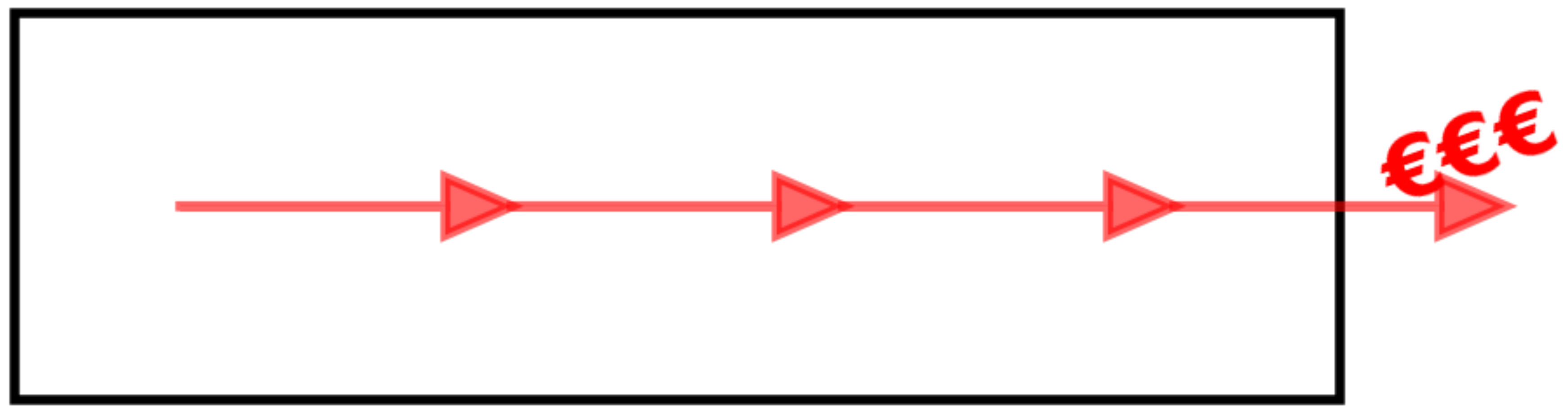

But high-field magnets are costly and hard to scale

Figure of merit

$$f \sim \left(B^2\, L^2\, A\right) \times \frac{\epsilon_d \epsilon_0}{\sqrt{ba}} \times \sqrt{\epsilon_t\, t}$$

Longer integration time (background-limited)

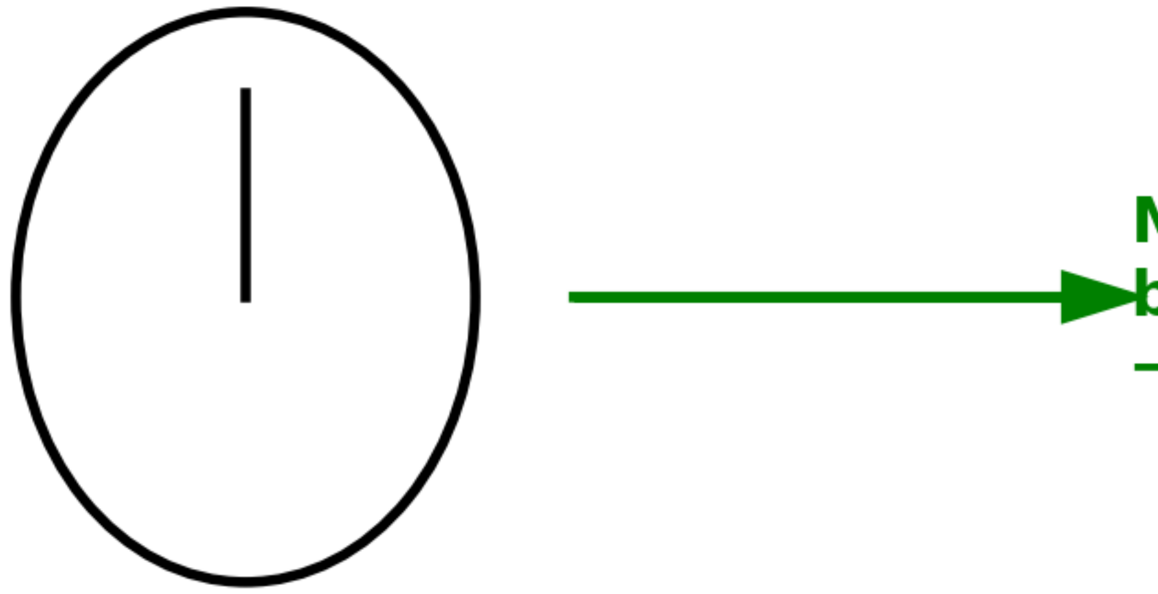

Longer integration time (background-free)

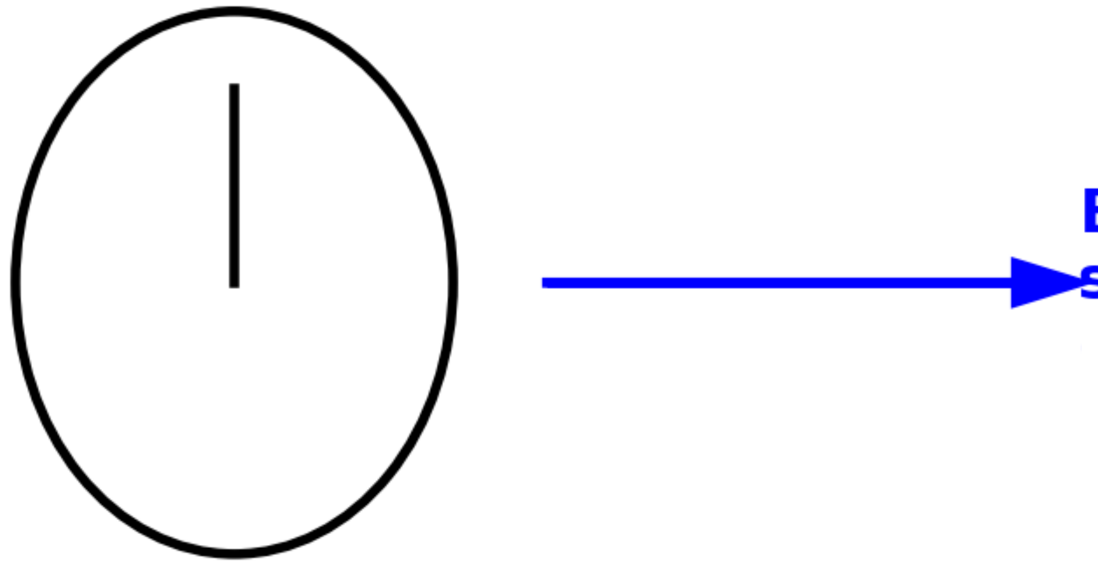

IAXO-International Axion Observatory

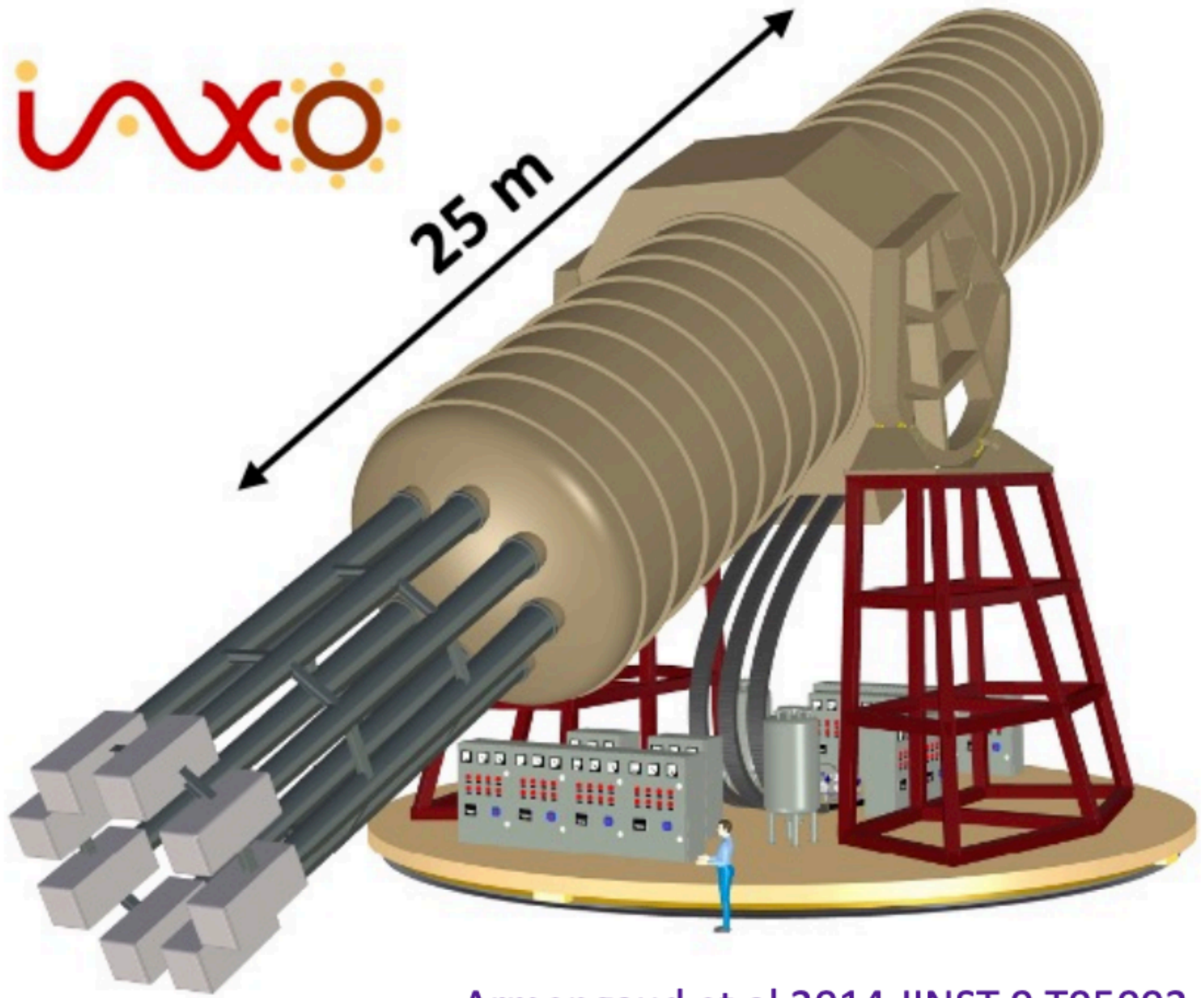

Armengaud et al 2014 JINST 9 T05002
Irastorza et al 2011 JCAP 1106, 013

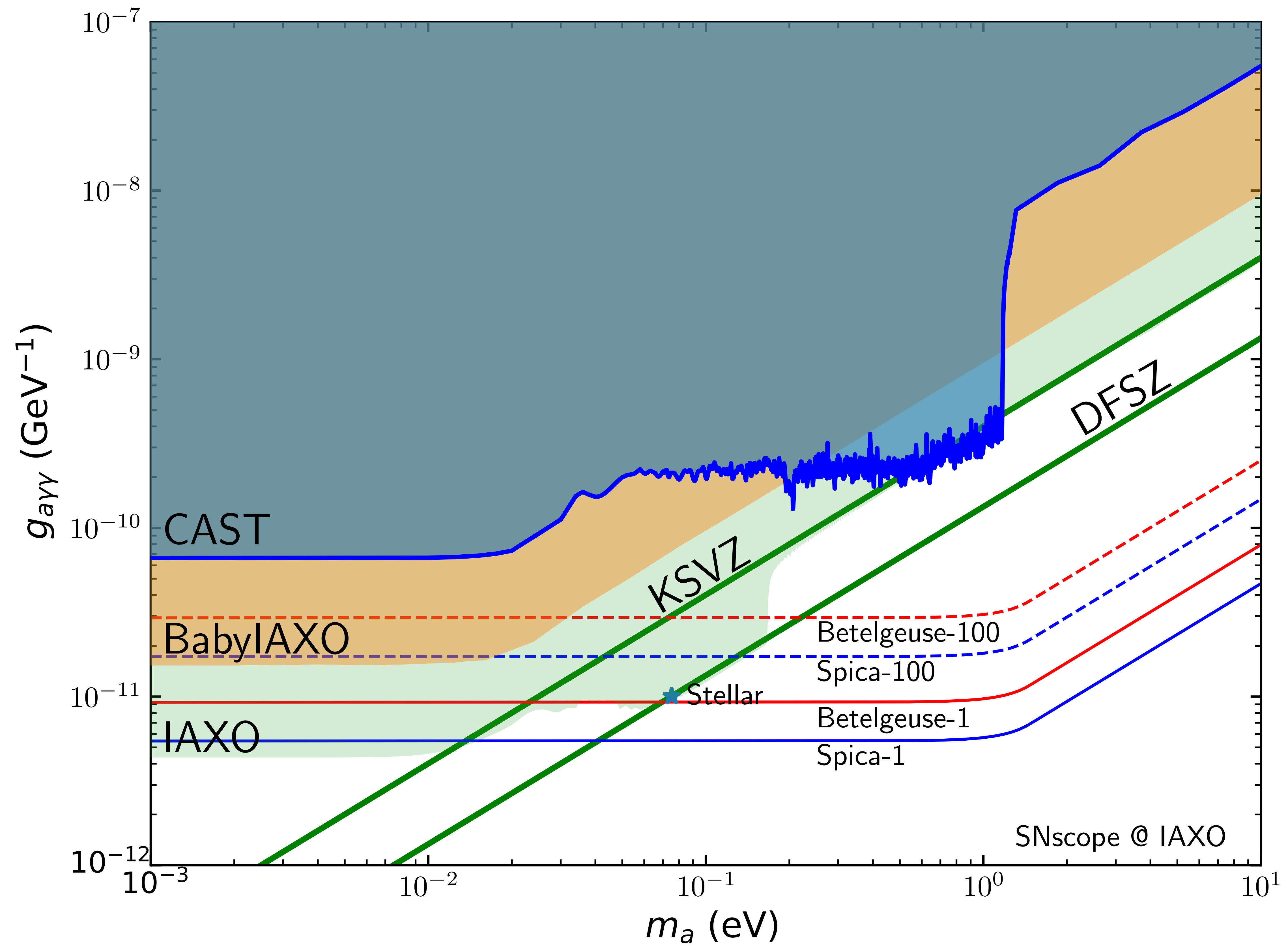

- Large toroidal 8-coil magnet L ≃ 20 m
- 8 bores: 600 mm diameter each
- 8 x-ray telescopes + 8 detection systems
- Rotating platform with services

The expected gain of IAXO over CAST is a factor of 10^4–10^5 in SNR

Solar tracking

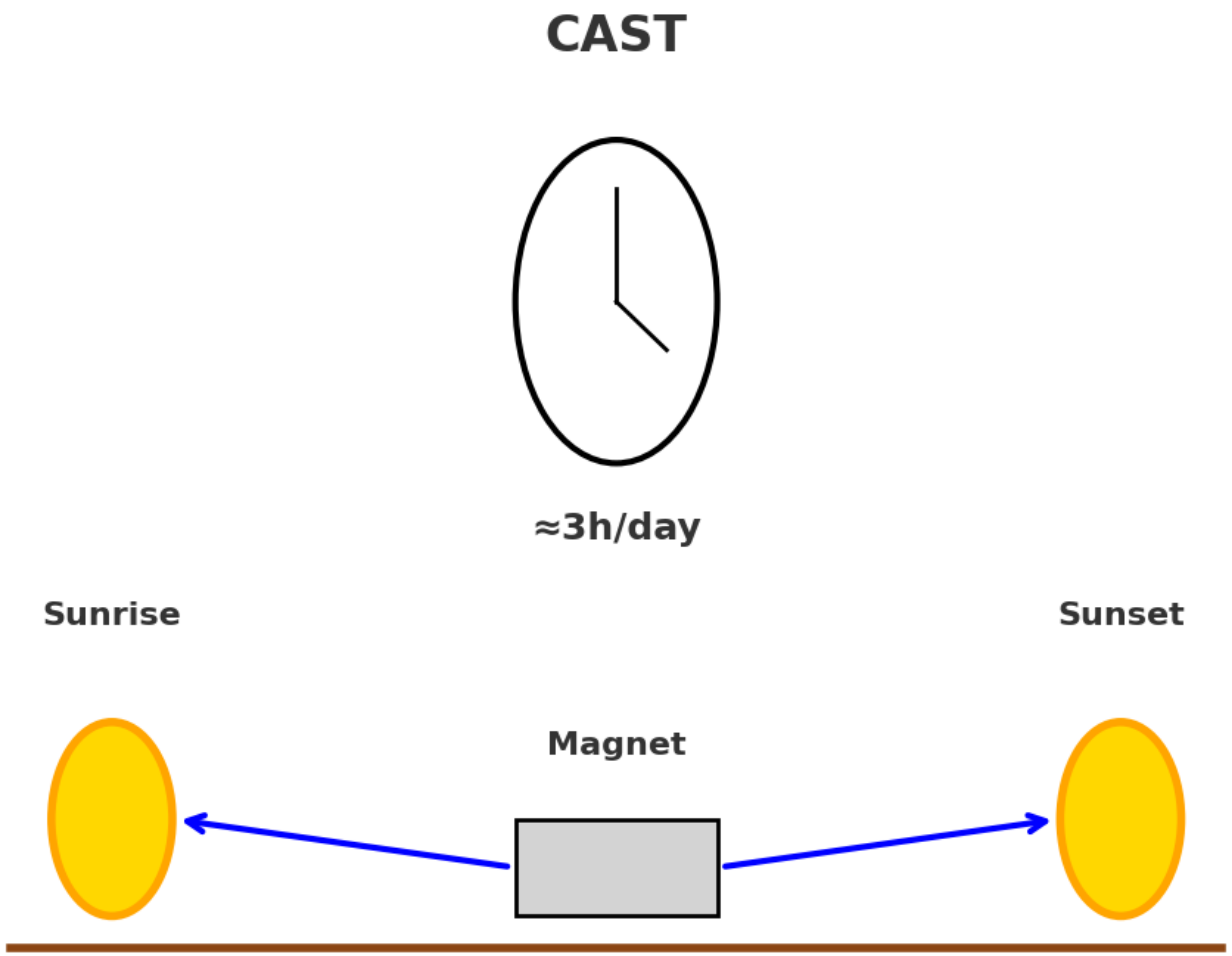

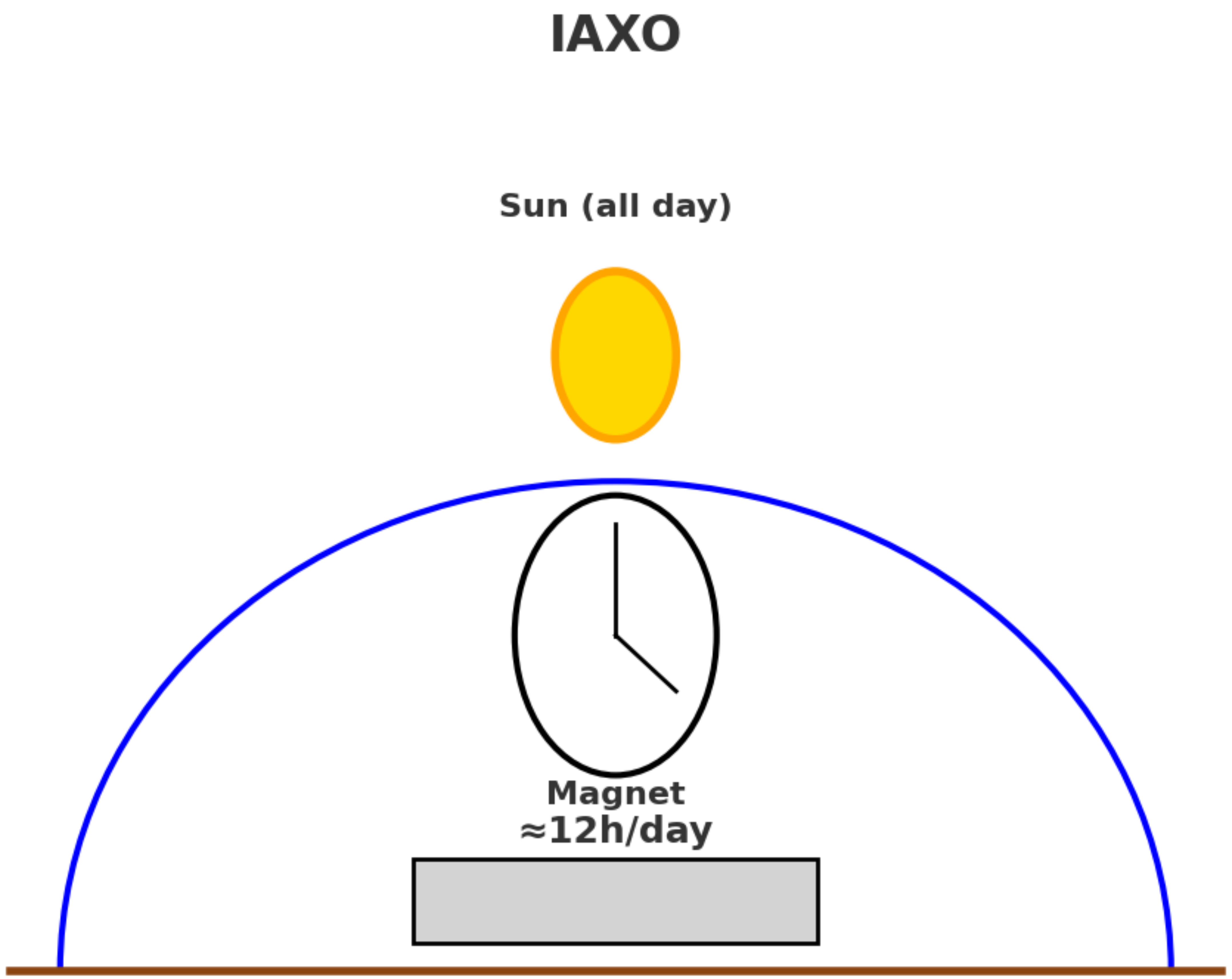

Fixed mount

Full azimuthal + elevation drive → continuous solar tracking

Tracking time ∝ exposure → sensitivity boost

Axion-electron couplings

Production

- ❖ ABC axions via axion-fermion couplings $\mathscr{L}_{aee} = g_{ae}\, a\, \bar{\psi}_e \gamma_5 \gamma^\mu \psi_e$
- ❖ Plasmon-ALP conversion in large-scale solar B-fields

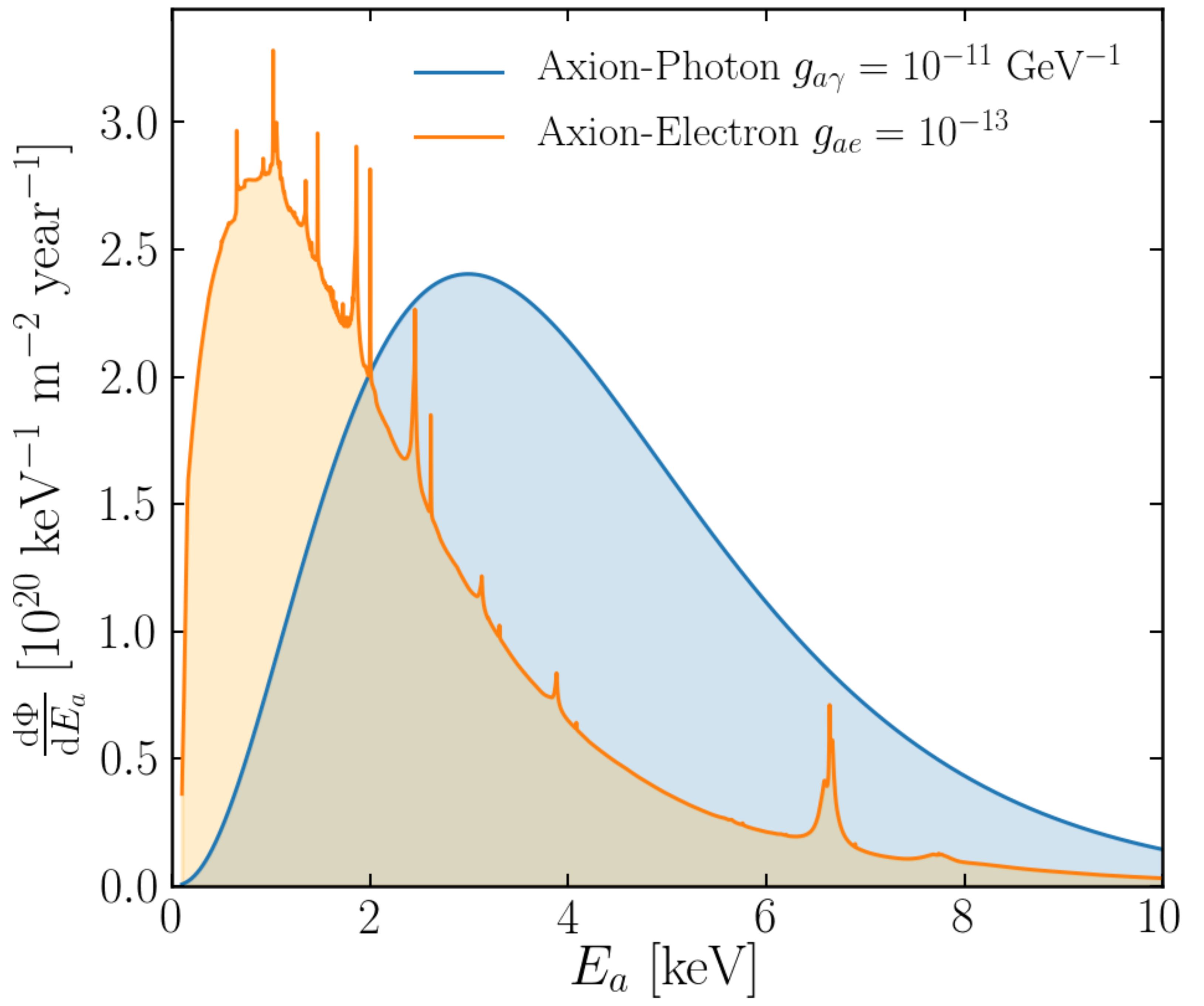

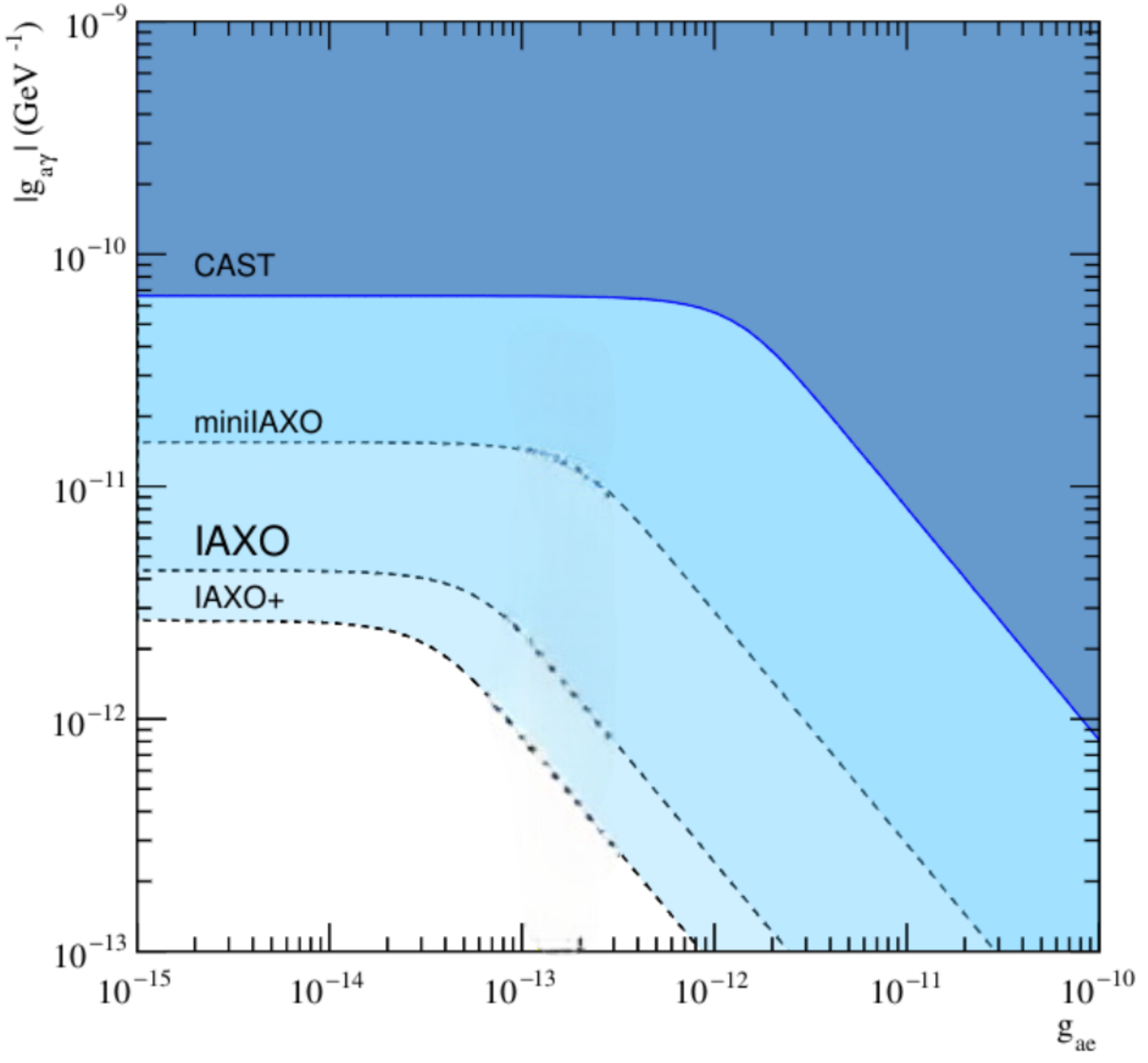

Detection

- ❖ Larger aperture (A) →higher acceptance
- ❖ Energy resolution to disentangle spectral features
- ❖ Low thresholds for soft axions (~10-100 eV)
- ❖ X-ray telescopes (XRTs)+detectors (Micromegas,cryogenic calorimeters)
  → Background suppression+spectral sensitivity

Axion-nucleon couplings

$$\mathcal{L}_{aN} = -ia\,\bar{N}\gamma_5\left(g^0_{aN} + g^3_{aN}\tau^3\right)N$$

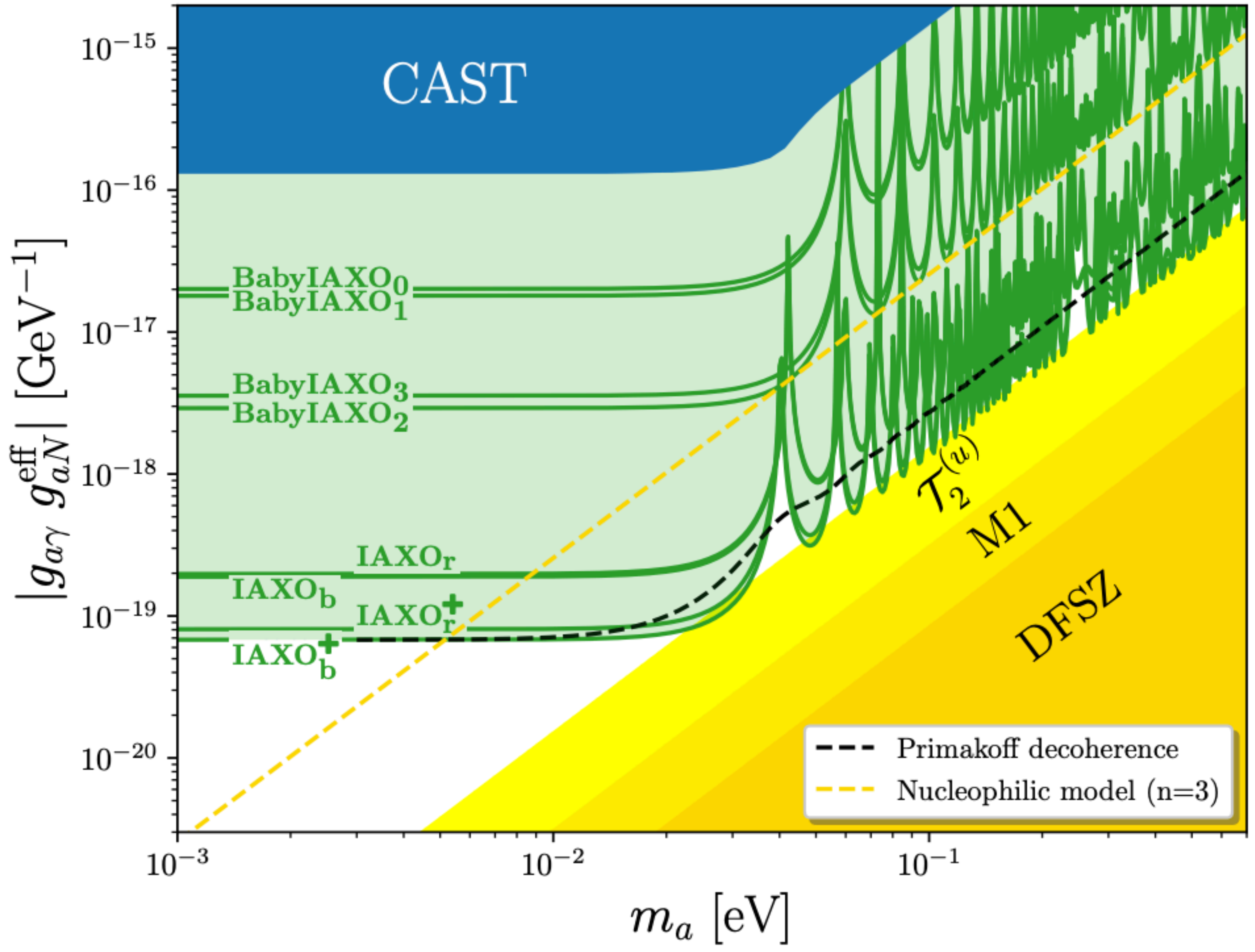

Di Luzio et. al., Eur. Phys. J. C 82, 120 (2022)

Production (^{57}Fe line, 14.4 keV)

- Nuclear M1 transition in 57Fe → monoenergetic 14.4 keV axions
- Axion-nucleon couplings unavoidable in QCD axion models
- Updated nuclear data → ~30% stronger emission rates
- Oscillatory signal at Earth from conversion probability $\propto \sin^2(qL/2)/(qL/2)^2$

Instrumentation

- X-ray optics not optimised above 10 keV→efficient drops
- Detectors need good energy resolution to isolate narrow line
- Primakoff continuum at 14 keV acts as background
- Candidate technologies:
  - Micromegas →low background
  - CZT/cryogenic detectors →better resolution and thresholds

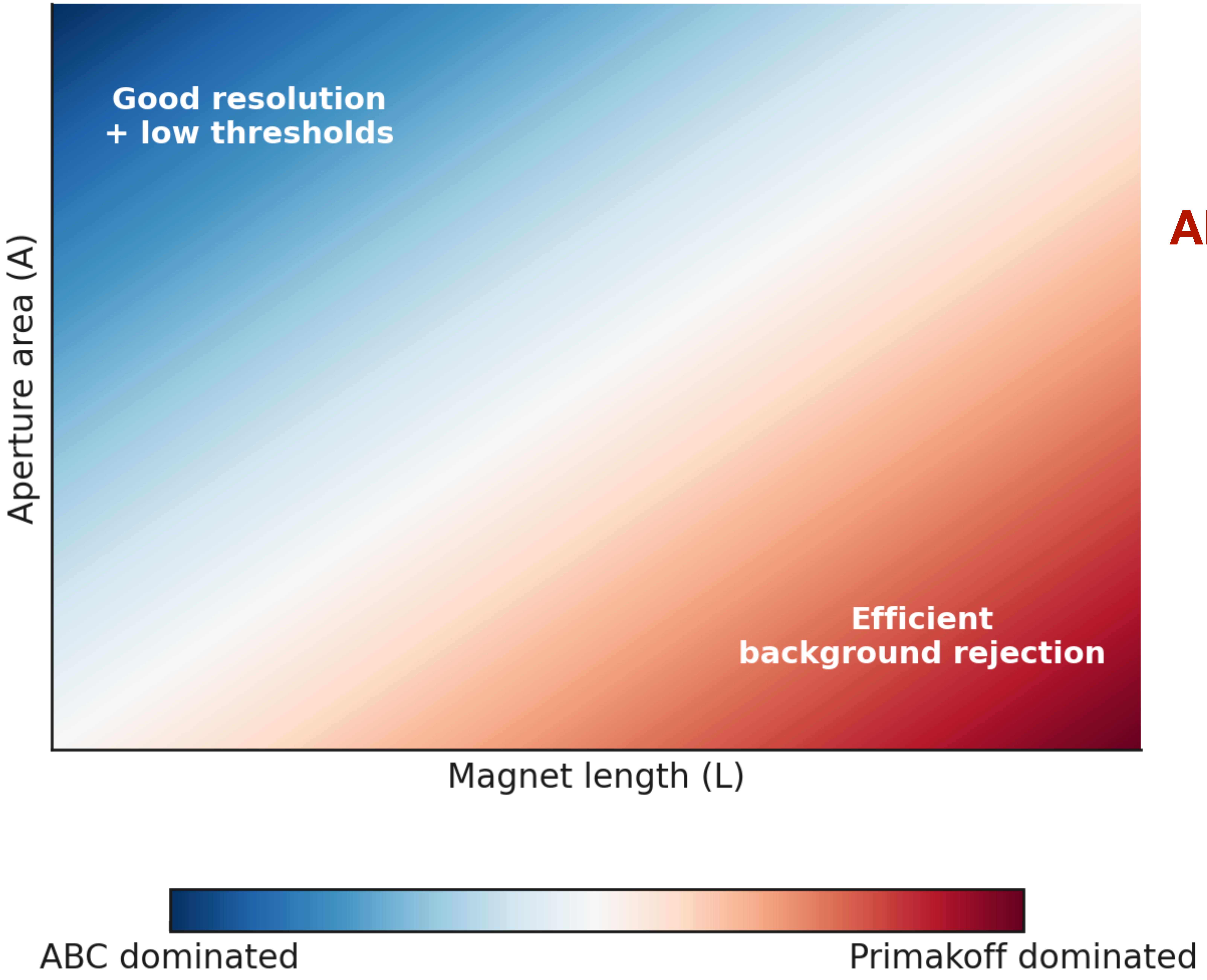

Generic model :

ALP can couple to anything.

How will you optimise then?

Larger area? Longer L?

Better resolution?

Thank you!!

ALP interactions at different scales

M. Bauer, *SC* and G. Rostagni, JHEP 05 (2025) 023

✓ ALPs at the UV scale

$$\mathcal{L}_{\text{eff}}^{D\leq 5}(\mu > \Lambda_{\text{QCD}}) \ni \frac{\partial^\mu a}{2f}\, c_{uu}\, \bar{u}\,\gamma_\mu \gamma_5\, u + \frac{\partial^\mu a}{2f}\, c_{dd}\, \bar{d}\,\gamma_\mu \gamma_5\, d + c_{GG}\frac{\alpha_s}{4\pi}\frac{a}{f} G_{\mu\nu}\tilde{G}^{\mu\nu} + \ldots$$

✓ RG running

✓ Threshold matching

$$\Sigma = \exp(i\sqrt{2}\Pi/f_\pi)$$

✓ Chiral Lagrangian

$$\mathcal{L}_{\chi\text{PT}} = \frac{f_\pi^2}{4}\text{tr}[\Sigma\, m_q(a)^+ + m_q(a)\Sigma^+]$$

Quark mass matrix is ALP-field dependent !!

$$m_q(a) = e^{-i\kappa_q \frac{a}{f} c_{GG}} m_q e^{-i\kappa_q \frac{a}{f} c_{GG}}$$

ALP linear interactions

At energy scales below Λ_{QCD}, the relevant ALP couplings to photons, nucleons and electrons are written in the leading order of the expansion of the decay constant f as

$$\boxed{\begin{aligned}\mathscr{L}_{\text{eff}}^{D\leq 5}(\mu \lesssim \Lambda_{\text{QCD}}) = \frac{1}{2}\left(\partial_\mu a\right)(\partial^\mu a) - \frac{m_{a,0}^2}{2}a^2 \\ + \frac{\partial^\mu a}{2f} c_{ee}\,\bar{e}\,\gamma_\mu\gamma_5\, e + g_{Na}\frac{\partial^\mu a}{2f}\bar{N}\gamma_\mu\gamma_5 N + c_{\gamma\gamma}^{\text{eff}}\frac{\alpha}{4\pi}\frac{a}{f}F_{\mu\nu}\tilde{F}^{\mu\nu}\end{aligned}}$$

$$c_{\gamma\gamma}^{\text{eff}}(\mu_0) = c_{\gamma\gamma}(\Lambda) - 1.92\, c_{GG}(\Lambda)$$